

AD-A142 293

A STUDY OF THE DEPENDENCE OF MICROSEGREGATION ON  
CRITICAL SOLIDIFICATION (U) UNITED TECHNOLOGIES  
RESEARCH CENTER EAST HARTFORD CT D B SNOW MAR 84

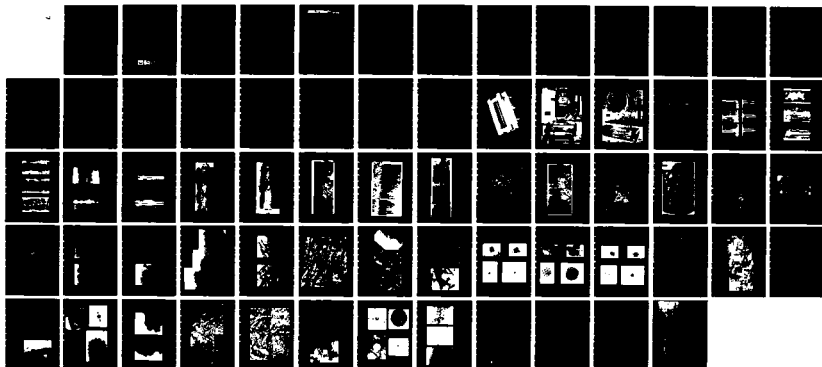
1/1

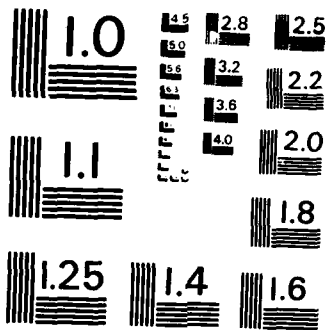
UNCLASSIFIED

UTRC/R84-915797-4 N00014-79-C-0649

F/G 11/6

NL





MICROCOPY RESOLUTION TEST CHART  
NATIONAL BUREAU OF STANDARDS-1963-A

R84-915797-4

①

# A STUDY OF THE DEPENDENCE OF MICROSEGREGATION ON CRITICAL SOLIDIFICATION PARAMETERS IN RAPIDLY- QUENCHED STRUCTURES

AD-A142 293

Prepared by  
D.B. Snow

Final Report

Contract N00014-79-C-0649  
Project No. NR 031-825/5-28-81 (471)

JUN 21 1994

for

Office of Naval Research  
Department of the Navy  
Arlington, Virginia 22217

by



**UNITED  
TECHNOLOGIES  
RESEARCH  
CENTER**

East Hartford, Connecticut 06108

DTIC FILE COPY

Reproduction in whole or in part is permitted for any purpose of the United States Government

84 06 20 038

REPORT DOCUMENTATION PAGE		READ INSTRUCTIONS BEFORE COMPLETING FORM
1. REPORT NUMBER R84-915797-4	2. GOVT ACCESSION NO. AD A142 293	3. RECIPIENT'S CATALOG NUMBER
4. TITLE (and Subtitle) A STUDY OF THE DEPENDENCE OF MICROSEGREGATION ON CRITICAL SOLIDIFICATION PARAMETERS IN RAPIDLY-QUENCHED STRUCTURES		5. TYPE OF REPORT & PERIOD COVERED FINAL REPORT Aug. 1979 - Mar. 1984
7. AUTHOR(s) D. B. Snow		6. PERFORMING ORG. REPORT NUMBER
9. PERFORMING ORGANIZATION NAME AND ADDRESS United Technologies Research Center East Hartford, CT 06108		8. CONTRACT OR GRANT NUMBER(s) N00014-79-C-0649
11. CONTROLLING OFFICE NAME AND ADDRESS Office of Naval Research Department of the Navy Arlington, VA 22217		10. PROGRAM ELEMENT, PROJECT, TASK AREA & WORK UNIT NUMBERS
14. MONITORING AGENCY NAME & ADDRESS (if different from Controlling Office)		12. REPORT DATE March 1984
		13. NUMBER OF PAGES 60
		15. SECURITY CLASS. (of this report) Unclassified
		15a. DECLASSIFICATION/DOWNGRADING SCHEDULE
16. DISTRIBUTION STATEMENT (of this Report) Distribution in whole or in part is permitted for any purpose of the United States Government <b>APPROVED FOR PUBLIC RELEASE DISTRIBUTION UNLIMITED</b>		
17. DISTRIBUTION STATEMENT (of the abstract entered in Block 20, if different from Report)		
18. SUPPLEMENTARY NOTES (approx. 50000 C/s)		
19. KEY WORDS (Continue on reverse side if necessary and identify by block number) Laser Welding                      Yttrium Oxide LAYERGLAZE Processing          Neodymium Oxide Titanium Martensite              Rapid Solidification Microsegregation                Rapid Solidification Technology Ti-6Al-4V                            As-Welded Mechanical Properties		
20. ABSTRACT (Continue on reverse side if necessary and identify by block number) Mechanically-blended powder alloys of Ti-6Al-4V, Ti-6Al-4V blended with $\leq 3\text{Er}$ , Y or Nd, and Ti-6Al-2Sn-4Zr-6Mo-1Er (wt%) were laser-consolidated and rapidly solidified ( $\sim 5 \times 10^4$ °C/s) by the LAYERGLAZE <sup>SM</sup> process. This procedure was used to form the fusion zones of butt welds in Ti-6Al-4V plate, premachined with straight-sided 3 mm gaps, which were filled with sequential layers of laser-melted powder feedstock. After melting, the rare-earth elements reacted with dissolved oxygen in the titanium to form a dispersion of equilibrium-structure oxides. The		

#19. Cont'd

Rare-Earth Element Alloying  
Rare-Earth Oxides  
Oxide Dispersion Strengthening  
Erbium Oxide

alpha

#20. Cont'd

as-solidified microstructure of each alloy consisted of large, columnar grains of acicular  $\alpha'$  HCP martensite. The largest rare earth oxide size and spatial dispersions were observed in alloys LAYERGLAZED from Ti-6Al-4V-3Nd powder; the finest, in those made from Ti-6Al-4V-1.5Er. The largest oxide particles were located at interdendritic and, in the case of Ti-6Al-4V-1.5Er, at intergranular sites. The erbium oxide size distribution was bimodal, with mean sizes of 280 and 40 nm. The oxide structures were identified by analysis of selected area and convergent beam diffraction patterns, obtained from particles determined to contain the appropriate rare earth element by EDS. Neither the ambient temperature tensile strength nor the microhardness of either aged (800°C, 75 min) or as-LAYERGLAZED alloys were significantly improved by the oxide dispersions. Presumably, this occurred because the anticipated dispersion strengthening was offset by the removal of oxygen from solid solution. However, the tensile ductility of Ti-6Al-4V was increased by the addition of yttrium. The 40 nm  $Er_2O_3$  particles observed in the alloy LAYERGLAZED from Ti-6Al-4V-1.5Er might be reasonably expected to improve creep strength.



A1

# UNITED TECHNOLOGIES RESEARCH CENTER



East Hartford, Connecticut 06108

R84-915797-4

A Study of the Dependence of Microsegregation  
on Critical Solidification Parameters in  
Rapidly-Quenched Structures

FINAL REPORT

Contract N00014-79-C-0649

REPORTED BY *D. B. Snow*

D. B. Snow

APPROVED BY *A. F. Giamei*

A. F. Giamei, Principal Scientist  
Alloy & Process Research

DATE March 1984

NO. OF PAGES \_\_\_\_\_

COPY NO. \_\_\_\_\_

TABLE OF CONTENTS

	<u>Page</u>
<b>INTRODUCTION</b> . . . . .	1
<b>EXPERIMENTAL PROCEDURE</b> . . . . .	2
A. Laser Processing . . . . .	2
B. Powder Feedstock . . . . .	2
C. Structure and Mechanical Properties . . . . .	3
<b>RESULTS</b> . . . . .	4
A. Chemical Analysis . . . . .	4
B. Tensile and Microhardness Data . . . . .	4
C. Macrostructure . . . . .	5
D. Microstructure, Conventional Metallography . . . . .	5
E. Aged Specimens . . . . .	6
F. Analytical Electron Microscopy . . . . .	6
G. Auger Electron Spectroscopy . . . . .	9
<b>DISCUSSION</b> . . . . .	10
<b>CONCLUSIONS</b> . . . . .	11
<b>ACKNOWLEDGEMENT</b> . . . . .	12
<b>REFERENCES</b> . . . . .	13
<b>FIGURES 1 - 47</b>	

A Study of the Dependence of Microsegregation of Critical  
Solidification Parameters in Rapidly Quenched Structures

## INTRODUCTION

During the four-year period of this contract, several different aspects of the microsegregation and microstructures produced by laser materials processing were investigated. In compliance with the instructions of the controlling office, the material contained in the three annual technical reports previously issued under this contract (Refs. 1-3) are not presented again here. In brief, the first of these modeled and experimentally determined the cooling rates associated with continuous, CO<sub>2</sub> laser welding, and examined the dependence of cracking on composition in laser-welded Ni-Al-Mo alloys (Ref. 1). The second annual technical report described the variation in continuous, CO<sub>2</sub> laser welding efficiency and fusion zone segregation on beam power and cladding thickness in stainless-clad AH32 carbon steel plate (Ref. 2). The third examined the structure and properties of narrow-gap butt welds formed by the powder-feed LAYERGLAZE<sup>SM</sup> process in Ti-6Al-4V plate (Ref. 3). The present report describes the results of the final year of research under this contract. In this study, the procedures described in Ref. 3 were utilized to alloy Ti-6-4 and Ti-6-2-4-6 powder feedstock with rare earth elements to create oxide dispersions in the LAYERGLAZE - processed fusion zones.

Titanium and titanium base alloys have been considered for several decades as potential candidates for dispersion strengthening by stable oxides, particularly rare earth oxides (Refs. 4-6). The relative insolubility of most rare earth elements in titanium (Ref. 7), together with their strong affinity for oxygen, have caused embrittling segregation (Ref. 8) and/or relatively coarse (> 260 nm) dispersions (Refs. 5,9) in conventionally-solidified Ti-rare earth alloys. However, rapidly solidified Ti-Er alloys have been observed to contain more refined, homogeneous second phase dispersions (Refs. 10-12), which have a significant strengthening effect (Ref. 9). The compounds which form the second phase dispersions in rapidly solidified Ti-Al-Y and Ti-Er alloys have been positively identified as Y<sub>2</sub>O<sub>3</sub> and Er<sub>2</sub>O<sub>3</sub>, respectively (Refs. 13-15). The Er<sub>2</sub>O<sub>3</sub> dispersion was reported to have good thermal stability at 700°C (Ref. 15). The present investigation was intended to demonstrate that similar rare earth oxide dispersions can be achieved in titanium base alloys by using mechanically blended powder as feedstock for narrow-gap laser butt welds (LAYERGLAZE/narrow-gap welding) (Ref. 16).

## EXPERIMENTAL PROCEDURE

### A. Laser Processing

The specific laser operating characteristics and apparatus used in this investigation were similar to those utilized in a previous study of the LAYERGLAZE/narrow-gap welding of Ti-6Al-4V (Ref. 16). The narrow-gap butt welds were made in 1.27 or 5.08 cm, mill-annealed, ELI Ti-6Al-4V plate. Specimen edges were premachined so that straight sided, 3 mm gaps were formed when two pieces were fitted together (Fig. 1). The sides of the weld gap were chemically cleaned just before welding in a solution of 30% nitric and 3% hydrofluoric acid, then rinsed with water and dried with forced air. Specimen warpage during welding was minimized by clamping each in a retention fixture (Fig. 2).

All 1.27 cm thick specimens welded with Ti-6Al-4V feedstock were processed with a continuous, cross-flow carbon dioxide laser, operated in the unstable resonator mode (annular beam energy cross-section). A 47 cm focal length copper mirror directed the laser beam downward toward the bottom of the weld gap, which was positioned 2.86 cm below its focal plane (Fig. 3). These conditions gave a 3.2 mm (defocused) beam spot diameter at the fusion zone surface. The laser beam power at the work station was 3.9 kW, so that the power per unit area at the fusion zone surface was  $48.5 \text{ kW/cm}^2$ , maintained by lowering the specimen height after every four deposited layers. The powder feedstock was transported from its reservoir to a point just ahead of the beam impingement point by vibration-assisted gravity flow (Ref. 16) while the specimen was traversed at 2.12 cm/s. Specimens were enclosed during welding in a chamber filled with helium flowing at  $5.7 \text{ m}^3/\text{h}$ , which had a narrow opening at its top to allow the beam to enter (Ref. 16).

Two groups of specimens were processed with a UTRC-developed, modular  $\text{CO}_2$  laser (Ref. 18): 5.08 cm plate (center gap closure, Fig. 1), welded with prealloyed Ti-6Al-4V powder feedstock; and 1.27 cm plate (bottom gap closure, Fig. 1), welded with Ti-6Al-2Sn-4Zr-6Mo-1Er. These specimens were LAYERGLAZED with the workstation shown in Fig. 4, using a focusing mirror with a 61 cm focal length and a (defocused) beam spot diameter of 3 mm. A modular, cross-beam, continuous  $\text{CO}_2$  laser with stable oscillator optics (Gaussian mode) (Ref. 18) was operated so as to achieve a beam power of 2.25 kW ( $32 \text{ kW/cm}^2$ ) at the specimen surface. The specimen traverse and powder feed procedures were those described previously.

### B. Powder Feedstock

Prealloyed Ti-6Al-4V powder without additional alloying elements was used for welds in both the 1.27 and 5.08 cm thick specimens to establish a basis of comparison with the results of previous research (Refs. 3,16). However, all of the alloys which contained rare earth elements were prepared as mechanically blended powder, and had the following nominal compositions: Ti-6Al-4V; Ti-6Al-4V + 1.5Er, or 3Nd; and Ti-6Al-2Sn-4Zr-6Mo-1Er (wt%). The characteristics of the component powders used to blend these feedstock compositions are described in Table I.

Table I

## Powder Feedstock Specifications

<u>Powder</u>	<u>Purity (wt%) (metallics)</u>	<u>Mesh Size</u>	<u>Source</u>
Ti-6Al-4V(prealloyed)	99.98	-35, +325	Nuclear Metals
Ti-6Al-4V(mech. blend)	99.95	-170, +325	Amerimet Corp.
Er, Y, Nd	99.9	-40	Research Chemicals
Ti	99.8	-170, +325	Alloy Metals
Al	99.5	-100, +325	CERAC
Sn	99.9	-170	Fisher Scientific
Zr	99.9	-80	Alfa Products
Mo	99.8	-100	A. D. MacKay

## C. Structure and Mechanical Properties

The as-LAYERGLAZED microstructure of each alloy was examined by light microscopy, TEM/STEM (Philips EM400T), electron microprobe analysis (Cameca - "CAMEBAX"), and scanning Auger electron spectroscopy (Perkin-Elmer PHI 600). As-processed fusion zone compositions were obtained by wet chemical analysis, inert gas fusion (Leco), and wavelength-dispersive X-ray spectroscopy (electron microprobe).

Tensile specimens were machined from the fusion zone of each of the alloys based on Ti-6-4 (Fig. 5). The load axis of each was oriented parallel to the welding direction, so that the gage section consisted entirely of LAYERGLAZE-processed material (Fig. 6). The diamond pyramid microhardness of each alloy was measured with a 200 g load on transverse cross-sections of the fusion zones.

As-LAYERGLAZED specimens of each alloy were heat treated at 800°C for 75 min in continuously-purified, flowing argon ( $<10^{-7}$  ppm O<sub>2</sub>) and furnace cooled.

## RESULTS

## A. Chemical Analysis

The results of the chemical analyses of the fusion zone of each alloy are shown in Table II. The microprobe results are assumed to be the most reliable, since standards of known composition were used, and the specimen surfaces were unetched. The results show that some loss of the alloying elements occurred during laser melting. This loss was somewhat more pronounced for those elements with relatively low melting points and for the rare earths.

Table II  
Chemical Analyses, As-LAYERGLAZED Alloys (wt%)

<u>Powder Composition</u>	<u>Al</u>	<u>V</u>	<u>Er</u>	<u>Y</u>	<u>Nd</u>	<u>O</u>	<u>C</u>	<u>Sn</u>	<u>Zr</u>	<u>Mo</u>
Ti-6Al-4V, prealloyed powder, Ref. 13	5.8	4.1	-	-	-	.14	ND*	-	-	-
Ti-6Al-4V, mech. blend	7.2	3.9	-	-	-	.13	.02	-	-	-
Ti-6Al-4V-1.5Er	6.4	4.0	>.2	-	-	.12	.02	-	-	-
Ti-6Al-4V-1.5Er**	4.8	4.1	0.7	-	-	ND	ND	-	-	-
Ti-6Al-4V-1.5Y	6.6	ND	-	<3	-	.10	.02	-	-	-
Ti-6Al-4V-3Nd	6.2	3.6	-	-	>.9	.26	ND	-	-	-
Ti-6Al-2Sn-4Zr-6Mo-1Er**	4.9	-	.9	-	-	ND	ND	.8	3.2	4.6

\*Not Determined

\*\*Electron Microprobe Data

## B. Tensile and Microhardness Data

The tensile properties and/or microhardness of the alloys were determined in the as-LAYERGLAZED condition, and in some cases after an aging heat treatment (800°C, 75 min) as well (Table III). Irregularly-distributed fusion zone porosity in the gage section of several tensile specimens invalidated their test results, and made the data in Table III less complete than anticipated.

Table III  
Tensile\* and Microhardness Data

Feedstock** Composition (wt%)	Processing History	0.2% YS MPa(ksi)	MPa(ksi)	% $\epsilon$	Microhardness, DPH, 200g load (mean, $\pm 2s$ )
Ti-6Al-4V	As-LAYER- GLAZED	931 (135)	1027 (149)	11	388 $\pm$ 26
Ti-6Al-4V-1.5Er		848 (123)***	876 (127)	9	376 $\pm$ 38
Ti-6Al-4V-1.5Er		945 (137)	1027 (149)	15	373 $\pm$ 20
Ti-6Al-4V-3Nd		938 (136)	965 (140)	3	382 $\pm$ 32
Ti-6246-1Er		-	-	-	381 $\pm$ 10
Ti-6Al-4V	Annealed, 800°C, 75 min	917 (133)	979 (142)	6	346 $\pm$ 10
Ti-6Al-4V-1.5Er		-	-	-	361 $\pm$ 22
Ti-6Al-4V-1.5Y		833 (128)	965 (140)	14	371 $\pm$ 18
Ti-6Al-4V-3Nd		910 (132)	945 (137)	6	374 $\pm$ 10

\*Load axis parallel to welding direction: 100% fusion zone gage section

\*\*Nominal composition, mechanically blended powder

\*\*\*Macroscopic fracture surface porosity

### C. Macrostructure

The macrostructure and fusion zone surfaces of LAYERGLAZE/narrow-gap welds in both 1.27 and 5.08 cm thick specimens are shown in Figs. 7-11. The only distinctive difference between these specimens and those previously LAYERGLAZED from prealloyed Ti-6Al-4V powder (Refs. 3,16) was the relatively dull appearance of the fusion zone free surface of specimens alloyed with rare earth elements (Figs. 8,9). Microstructural analysis (subsequently presented) suggests that this was due to the presence of rare earth oxide particles.

### D. Microstructure, Conventional Metallography

Examination of the as-processed fusion zone microstructures of all specimens by conventional metallography (Figs. 12-23) revealed the columnar grain structure previously described in similar Ti-6Al-4V specimens (Refs. 3,16), and typical of LAYERGLAZE processing in general (Ref. 18). These grains were formed by sequential epitaxial nucleation at the interface of each layer as it solidified (Figs. 10, 12 - 16,18,20). The 5.08 cm specimen was welded by LAYERGLAZING 2.5 cm deep gaps from each side, and displayed some of the large porosity and incompletely-filled fusion zone areas observed similarly-processed 1.27 cm thick specimens (Figs. 12,13). Although the fusion zone grain structures formed by each alloy were quite similar, a greater amount of macroscopic porosity was observed in those which contained a rare earth element. This effect was particularly evident in the fusion zones LAYERGLAZED from Ti-6Al-4V-3Nd and Ti-6246-1Er powder (Figs. 20-22). In the latter case, the different sizes and shapes of the constituent powders caused intermittent blockage of the feedstock flow, so that previously-deposited layers in the fusion zone were often remelted.

Examination of the as-LAYERGLAZED specimens at higher magnification revealed a fully martensitic microstructure (Figs. 17,19,21,23) with no evidence of grain boundary precipitation, as described in detail in Refs. 3 and 16. Also visible were small (0.5-1.6  $\mu\text{m}$ ) particles, subsequently identified as rare earth oxides. These were distributed entirely in interdendritic rows in the specimen LAYERGLAZED from Ti-6Al-4V-1.5Y (Fig. 19), and with both random and interdendritic distribution in the case of the alloys to which Nd or Y had been added (Figs. 17,21).

#### E. Aged Specimens

Specimens cut from the as-LAYERGLAZED Ti-6Al-4V base specimens were aged at 800°C for 75 min in an attempt to determine whether additional rare earth oxide precipitation would occur. No evidence for additional dispersion strengthening was apparent in the tensile test data (Table III), although the alloys with rare earth additions were somewhat harder after aging than the Ti-6Al-4V alone (Table III). Metallographic observation of these specimens revealed only martensite and coarsening in the case of Ti-6Al-4V, and some precipitation at grain boundaries in the Ti-6Al-4V specimens which had been alloyed with rare earth elements (Figs. 24,25). Previously published results indicated that some Er supersaturation could be anticipated (Ref. 15), but difficulty in TEM specimen preparation from LAYERGLAZED and aged Ti-6Al-4V + Er samples has not as yet allowed a search for the very fine  $\text{Er}_2\text{O}_3$  precipitation that may have resulted.

#### F. Analytical Electron Microscopy

The second phase dispersions in the as-LAYERGLAZED Ti-6Al-4V base alloys were examined by both conventional and scanning transmission electron microscopy. The annular dark field STEM mode was used with a camera constant chosen to suppress Bragg contrast from the martensitic matrix (e.g., Figs. 26,27), and thus reveal the particle distribution more clearly than in a CTEM bright field image. Specimens as-LAYERGLAZED from Ti-6Al-4V + 1.5Er powder contained a bimodal second phase dispersion (Figs. 26,27), with irregularly-shaped particles of 28 nm mean size present at grain boundaries and at random locations within the grains, and some suggestion of interdendritic precipitation (left side of Fig. 26). At higher magnifications, numerous fine, 40 nm precipitates were observed throughout the microstructure (Figs. 27,28). Stereoscopic imaging revealed that some of the rows of fine particles shown in Figs. 27,28 were in fact planar arrays (Fig. 29). This observation suggests either precipitation at martensite plate boundaries or between secondary dendrite arms. The 40 nm particles did not all precipitate with the same orientation, even within the same martensite plate, and so only a few were in contrast at the same time in conventional dark field images. However, backscattered electron STEM images of areas previously photographed in the annular dark field STEM mode (Fig. 29) showed that all particles contained an element of high atomic number (Er).

Energy-dispersive X-ray spectra were used to confirm that the particles shown in Figs. 26-29 contained Er. An example of such data is presented in Fig. 30, taken in the STEM mode at 120 kV with a 5 nm nominal beam diameter and a 480s live counting time. The smaller particles in this specimen of as-LAYERGLAZED Ti-6Al-4V + Er are shown to produce an X-ray spectrum similar to that from one of the large ones. When the orientation of particles near the foil edge was favorable for diffraction analysis, selected area and convergent beam diffraction patterns were obtained from a particular particle first, then EDS was used to confirm that it contained the appropriate rare earth element.

The crystal structure of each of the three rare earth oxide particles observed in the alloys based on Ti-6Al-4V was determined by quantitative analysis of selected area diffraction patterns, rather than by point and space group identification from convergent beam diffraction patterns as in previous investigations Refs. 13,14. The oxides remained much thicker than the surrounding martensite after electropolishing, so that only those near or at the foil edge were thin enough for detailed study. Interplanar spacings were calculated from selected area diffraction patterns or major zone axes. The diffraction spots from the adjacent martensite, previously determined to have lattice parameters of  $a_0 = 2.93\text{\AA}$  and  $c_0 = 4.675\text{\AA}$  in these specimens, were used to calculate the camera constant of each individual pattern. In the case of  $\text{Er}_2\text{O}_3$  and  $\text{Y}_2\text{O}_3$ , the  $[100]$ ,  $[110]$ , and  $[\bar{1}11]$  zone axis patterns were obtained; for  $\text{Nd}_2\text{O}_3$   $[0111]$  and  $[121\bar{3}]$  were used. The observed lattice spacings agreed with those calculated from the lattice parameters of the equilibrium oxide structures to within  $\pm 0.02\text{\AA}$  (Tables IV-VI). Diffraction patterns from the three major zone axes of  $>100\text{\AA}$   $\text{Er}_2\text{O}_3$  particles in specimens as-LAYERGLAZED from Ti-6Al-4V-1.5Er powder are shown in Figs. 31-33. The strong intensities of the fourth order reflections in the convergent beam diffraction patterns are consistent with diffraction from a crystal structure which has space group  $I(2_1/a)3$ , as noted by Ref. 14.

In contrast to the bimodal oxide size distribution observed in the Ti-6-4 - Er alloy, the  $\text{Y}_2\text{O}_3$  particles in as-LAYERGLAZED Ti-6Al-4V + Y were observed to be 200-300 nm in size, and to have precipitated only between the primary dendrites (Figs. 34-36). No significant quantity of particles of  $<60$  nm were detected. EDS and diffraction data similar to those obtained from erbia are presented in Figs. 37-38.

The largest rare earth oxide particles ( $<600$  nm) were present in the specimens as-LAYERGLAZED from Ti-6Al-4V-3Nd, and these had a pronounced interdendritic and intergranular distribution (Figs. 39-41). A few areas of  $\text{Nd}_2\text{O}_3$  of  $<100$  nm size occurred (Fig. 39), but in general the martensite between the interdendritic rows did not contain precipitates. As with the other specimens, EDS was used to confirm the presence of Nd in a particular particle (Fig. 42); and whenever possible that particle was also analyzed by selected area and convergent beam diffraction (Fig. 43).

Table IV

Selected Area Diffraction Data:  $\text{Er}_2\text{O}_3$  in as-LAYERGLAZED Ti-6Al-4V

hkl	Calculated Interplanar Spacings ( $\text{\AA}$ )*	Observed Interplanar Spacings ( $\text{\AA}$ ) for Zone Axes:		
		$[001]$	$[011]$	$[\bar{1}11]$
01 $\bar{1}$	7.46	-	7.47	7.48
200	5.27	5.28	5.30	-
211	4.31	-	4.32	4.30
220	3.73	3.73		

\*Equilibrium Structure  $\text{Er}_2\text{O}_3$ :  $a_0 = 10.547\text{\AA}$ ; C- $\text{M}_2\text{O}_3$  Structure;  
Strukturbericht  $D5_3$ ; Space Group  $I(2_1/a)3 (Ia3)$

Table V

Selected Area Diffraction Data:  $Y_2O_3$  in as-LAYERGLAZED Ti-6Al-4V

hkl	Calculated Interplanar Spacings (Å)*	Observed Interplanar Spacings (Å) for Zone Axes:		
		$[00\bar{1}]$	$[011]$	$[\bar{1}11]$
$01\bar{1}$	7.48	-	7.47	7.48
200	5.29	5.30	5.30	-
$21\bar{1}$	4.32	-	4.32	4.34
220	3.74	3.75	-	-
310	3.35	3.36	-	-
$22\bar{2}$	3.05	-	3.05	-

\*Equilibrium Structure  $Y_2O_3$ :  $a_0 = 10.58\text{Å}$ ; C- $M_2O_3$  Structure;  
Strukturbericht  $D5_3$ ; SpaceGroup  $I(2_1/a)3, (Ia3)$

Table VI

Selected Area Diffraction Data:  $Nd_2O_3$  in as-LAYERGLAZED Ti-6Al-4V

hkl	Calculated Interplanar Spacings (Å)*	$[01\bar{1}1]$ $[0111]$ $[\bar{1}21\bar{3}]$		
		$10\bar{1}0$	3.33	-
$1\bar{1}01$	2.91	2.91	-	-
1011	2.91	2.92	-	-
$011\bar{1}$	2.91	-	-	2.90
$0\bar{1}12$	2.23	2.22	-	-
$\bar{2}\bar{1}10$	1.92	1.92	-	-
$11\bar{2}\bar{1}$	1.83	-	-	1.83

\*Equilibrium Structure  $Nd_2O_3$ :  $a_0 = 3.84\text{Å}$ ,  $c_0 = 6.00\text{Å}$ ;  
A- $M_2O_3$  Structure; Strukturbericht  $D5_2$ ; Space Group  $P3m1$

$Er_2O_3$  particle distributions similar to those described in Ti-6Al-4V + Er were observed in the alloy LAYERGLAZED from Ti-6Al-2Sn-4Zr-6Mo-1Er powder (Figs. 44,45). 200-400 nm erbia appeared at grain boundaries, and more randomly throughout the  $\alpha'$  HCP martensitic microstructure (Fig. 44). 40-60 nm particles were also present, and had a spatial dispersion and characteristic X-ray spectrum very similar to those observed in Ti-6Al-4V + Er (Fig. 45). No evidence for the interdendritic segregation of the other alloying elements was found, as exemplified by the Mo L $\alpha$  X-ray map shown in Fig. 44.

### G. Auger Electron Spectroscopy

Auger electron spectra were obtained with a 100 nm stationary beam from the sputter-cleaned surfaces of a specimen as-LAYERGLAZED from Ti-6Al-4V-1.5Er. The AES data from a 200 nm interdendritic  $\text{Er}_2\text{O}_3$  particle and the adjacent matrix are shown in Fig. 46. The  $\alpha'$  Ti-6-4 martensite contained some dissolved oxygen and carbon, as expected in this alloy (Fig. 46a), but no carbon signal was detected from the  $\text{Er}_2\text{O}_3$  particle itself (Fig. 46b). Unfortunately, it was not possible to determine with certainty whether or not the Ti peaks in Fig. 46b actually came from the surrounding matrix. Also, no information could be obtained concerning the incorporation of Al in the  $\text{Er}_2\text{O}_3$ , due to the overlap of the Er and Al signals in the range of 1393-1396 eV. A similar Auger spectrum was obtained from a 250 nm  $\text{Er}_2\text{O}_3$  particle in a carbon extraction replica taken from a specimen as-LAYERGLAZED from Ti-6Al-2Sn-4Zr-6Mo-1Er powder (Fig. 47). The results are essentially the same as for erbia in Ti-6Al-4V (Fig. 46b), save for the presence of a strong carbon peak, an artifact produced by the replicating material.

## DISCUSSION

This study represents a preliminary examination of the potential of rapid solidification technology, and specifically laser processing, for the creation of ODS titanium alloys. The rare earth oxide dispersions observed here were comparable to those reported in other titanium base alloys which had been rapidly solidified by laser processing (Refs. 12-15). The previous identification of these second phases as equilibrium-structure rare earth oxides (Refs. 13-15) was confirmed by quantitative analysis of selected area diffraction patterns from  $\text{Er}_2\text{O}_3$  and  $\text{Y}_2\text{O}_3$ . The tensile and microhardness data reflected a balance between the removal of oxygen from solid solution by rare earth oxide formation and the strengthening from the dispersion thus formed (Ref. 19). Quantitative evaluation of the alloy strength increase due to the dispersion would have been more accurately achieved at elevated temperature, where the effects of interstitial content and martensitic microstructure are not present.

Of the three rare earth elements added to Ti-6Al-4V in this investigation, only Er formed a fine dispersion (40 nm) of oxide particles within the dendrites, rather than between them. The randomly-oriented rows in which some of these were aligned (Figs. 27-29) suggested that they may have precipitated from solid solution at martensite plate boundaries. A similar observation has been reported in laser-melted Ti-Er (Ref. 15). These results, together with the observation of a bimodal dispersion of Er-rich particles in the alloy LAYERGLAZED from Ti-6246-1Er, indicate that oxide dispersion strengthening via erbium alloying and rapid solidification can be achieved in many commercial titanium alloys.

## CONCLUSIONS

1. Good chemical homogeneity ( $\mu\text{m}$  scale) was observed in specimens LAYERGLAZED from Ti-6Al-4V-1.5Er and Ti-6Al-2Sn-4Zr-6Mo-1Er. Some loss of alloying elements was observed, particularly for Sn and Er.
2. The primary dendrite spacing of 2-3  $\mu\text{m}$  which was observed in all as-processed alloys indicated an approximate cooling rate during solidification of  $\sim 5 \times 10^4$   $^{\circ}\text{C/s}$ .
3. The addition of Er, Y, or Nd to the Ti-6Al-4V powder feedstock increased the amount of macroscopic fusion zone porosity observed after LAYERGLAZE processing.
4. Rare earth elements react with the oxygen dissolved in titanium to form dispersed, equilibrium-structure oxides during LAYERGLAZE processing.
5. Oxide particle size and spatial distribution were coarsest for  $\text{Nd}_2\text{O}_3$ ; finest for  $\text{Er}_2\text{O}_3$  (bimodal distribution with 280 nm and 40 nm mean sizes in Ti-6Al-4V).
6.  $\text{Er}_2\text{O}_3$  particles were observed in specimens as-LAYERGLAZED from Ti-6246-1Er, with a similar distribution and lower quantity than in specimens LAYERGLAZED from Ti-6-4-1.5Er.
7. The rare earth oxide dispersions did not improve the ambient temperature tensile properties of as-LAYERGLAZED or aged Ti-6Al-4V. However, the 40 nm  $\text{Er}_2\text{O}_3$  could be expected to improve creep strength. Tensile ductility was increased in both as-processed and aged alloys consolidated from Ti-6Al-4V-1.5Y.

### ACKNOWLEDGEMENT

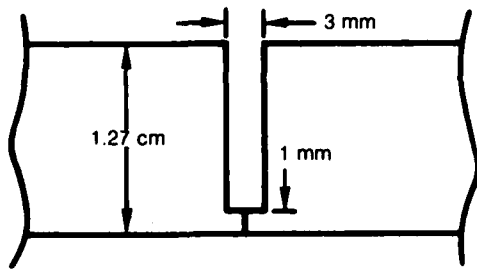
I would like to acknowledge the assistance of Mr. Raymond F. Duhamel with the laser processing, the preparation of thin foils by Mr. Gerald McCarthy, and many helpful discussions with Dr. Warren Oliver.

## REFERENCES

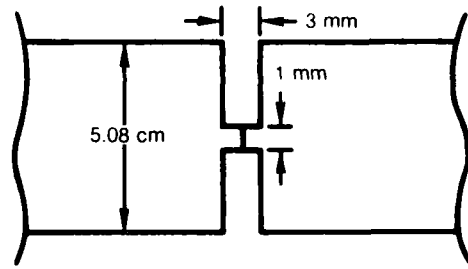
1. L. E. Greenwald, H. L. Fraser, M. J. Kaufman, and E. M. Breinan: A Study of the Dependence of Microsegregation on Critical Solidification Parameters in Rapidly-Quenched Structures, UTRC Annual Technical Report R80-914763-3, ONR Contract N00014-79-C-0649, Dec. 1980.
2. D. B. Snow, L. E. Greenwald, and E. M. Breinan: A Study of Microsegregation on Critical Solidification Parameters in Rapidly-Quenched Structures, UTRC Annual Technical Report R82-914763-6, ONR Contract N00014-79-C-0649, Jan. 1982.
3. E. M. Breinan and D. B. Snow: A Study of the Dependence of Microsegregation on Critical Solidification Parameters in Rapidly-Quenched Structures, UTRC Annual Technical Report R82-915797-2, ONR Contract N00014-79-C-0649, Oct. 1982.
4. R. H. Hiltz, Jr. and N. J. Grant: The Elevated Temperature Characteristics of Internally Oxidized Titanium-Cerium Alloys, Trans. TMS-AIME, 1958, vol. 212, pp 383-387.
5. C. F. Dixon and H. M. Skelly: Dispersion Strengthening Titanium with Refractory Oxides, Canadian Metall. Quart., 1972, vol. 11, pp 491-495.
6. R. C. Waugh: Suitable Oxides for Dispersion Strengthening of Titanium Alloys, International J. Powder Met. & Powder Tech., 1976, vol. 12, pp 85-89.
7. S. M. L. Sastry, T. C. Peng, and J. E. O'Neal: Dispersion Strengthened Powder Metallurgy Titanium Alloys, McDonnell Douglas Research Laboratories Interim Report MDC Q0741, Contract F33615-81-C-5011, July 29, 1981.
8. R. P. Simpson: Controlled Weld-Pool Solidification Structure and Resultant Properties with Yttrium Inoculation of Ti-6Al-4V-2Sn Welds, Welding J., 1977, vol. 56, no. 3, pp 67s-77s.
9. K. K. Sankaran, S. M. L. Sastry, and P. S. Pao: The Effects of Second-Phase Dispersoids on the Deformation Behavior of Titanium, Met. Trans. A, 1980, vol. 11A, pp 196-198.
10. B. B. Rath, J. E. O'Neal, and R. J. Lederich: Grain Refinement in Titanium - Erbium Alloys, Proc., Thirty-Second Annual Meeting, EMSA, G. W. Bailey, ed., Claitor's Publishing Div., Baton Rouge, 1974, pp 522-523.
11. S. M. L. Sastry, T. C. Peng, P. J. Meschter, and J. E. O'Neal: Rapid Solidification Processing of Titanium Alloys, J. Metals, 1983, vol. 35, no. 9, pp 21-28.
12. T. C. Peng, S. M. L. Sastry, and J. E. O'Neal: Exploratory Study of Laser Processing of Titanium Alloys, Lasers in Metallurgy, K. Mukherjee and J. Mazumder, eds., AIME, New York, 1981, pp 279-292.

13. D. G. Konitzer and H. L. Fraser: An Example of the Use of Combined Techniques of Analytical Transmission Electron Microscopy for Phase Identification, Microbeam Analysis - 1982, K. F. J. Heinrich, ed., San Francisco Press, San Francisco, 1982, pp 393-398.
14. D. G. Konitzer, B. C. Muddle, and H. L. Fraser: A Comparison of the Microstructures of As-Cast and Laser Surface Melted Ti-8Al-4Y, Met. Trans. A, 1983, vol. 14A, pp 1979-1988.
15. D. G. Konitzer, B. C. Muddle, and H. L. Fraser: Formation and Thermal Stability of an Oxide Dispersion in a Rapidly Solidified Ti-Er Alloy, Scripta Met., 1983, vol. 17, pp 963-966.
16. E. M. Breinan and D. B. Snow: Powder-Feed LAYERGLAZE/Narrow-Gap Laser Welding of Titanium-6Al-4V, Lasers in Materials Processing, E. A. Metzbower, ed., American Society for Metals, Metals Park, OH, 1983, pp 255-264.
17. E. M. Breinan, D. B. Snow, C. O. Brown, and B. H. Kear: New Developments in Laser Surface Melting Using Continuous Prealloyed Powder Feed, Rapid Solidification Processing, Principles and Technologies, II, R. Mehrabian, B. H. Kear and M. Cohen, eds., Claitor's Publishing Div., Baton Rouge, 1980, pp 440-452.
18. R. F. Duhamel and C. M. Banas: Laser Welding of Steels and Nickel Alloys, ibid., pp 209-216.
19. K. K. Sankaran, S. M. L. Sastry, and P. S. Pao: The Effects of Second-Phase Dispersoids on the Deformation Behavior of Titanium, Met. Trans. A, 1980, vol. 11A, pp 196-198.

**NARROW GAP WELD SPECIMEN CONFIGURATIONS**

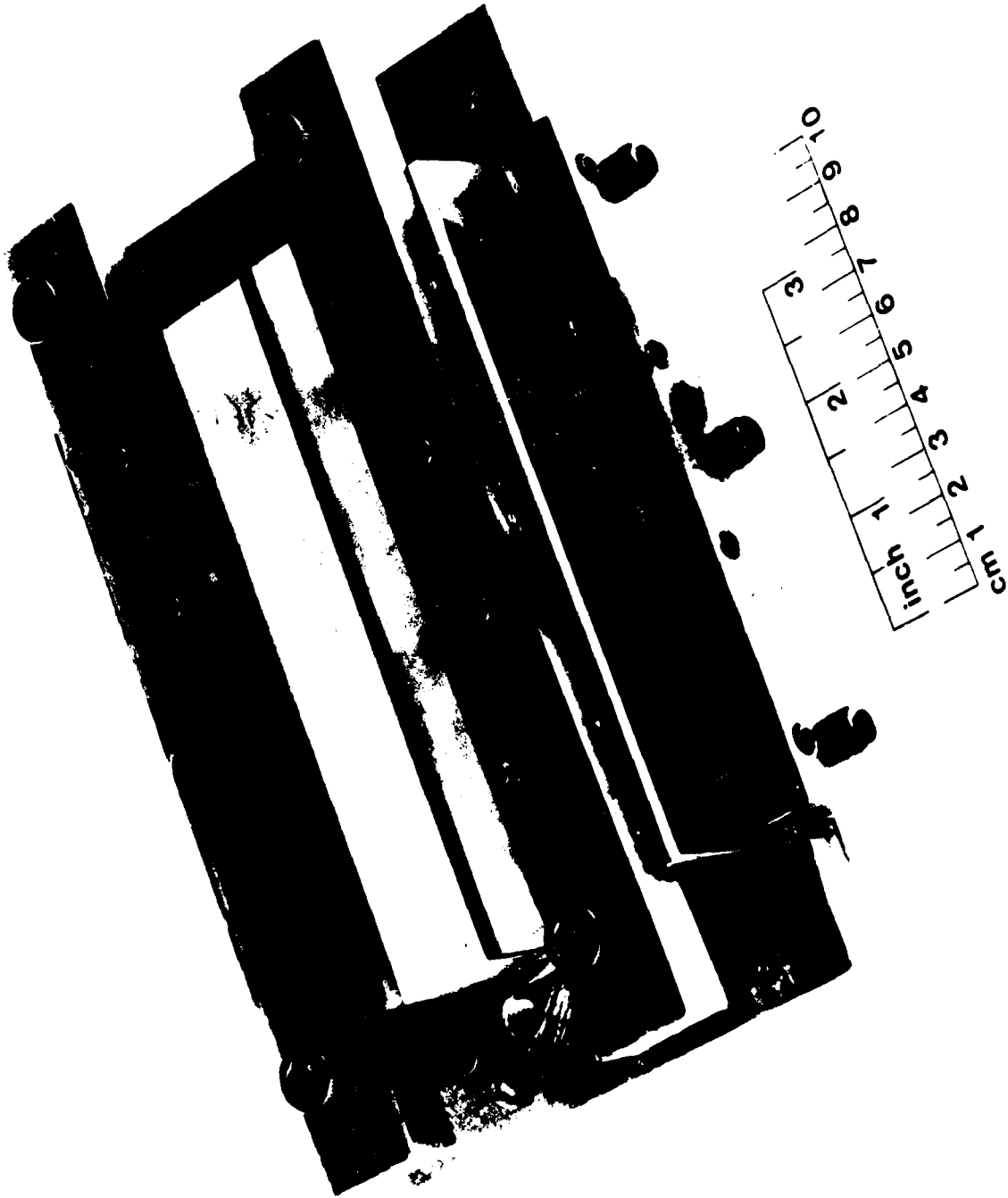


**BOTTOM CLOSURE**



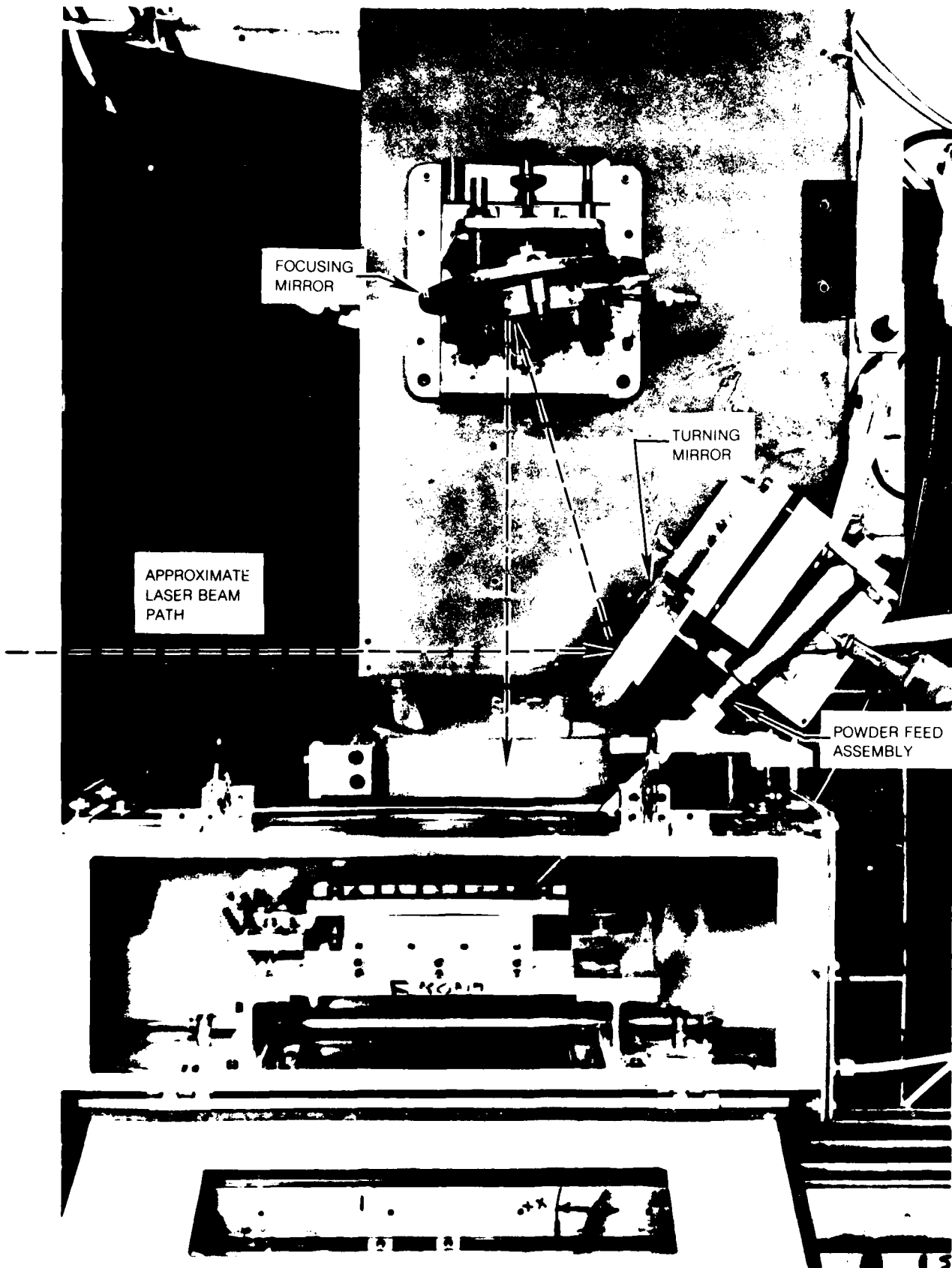
**CENTRAL CLOSURE**

**NARROW GAP WELD SPECIMEN POSITIONING FIXTURE**



# LAYERGLAZE WORK STATION FOR 1.27-cm Ti-6Al-4V PLATE

PROTECTIVE ATMOSPHERE CHAMBER DOOR OPEN



APPROXIMATE  
LASER BEAM  
PATH

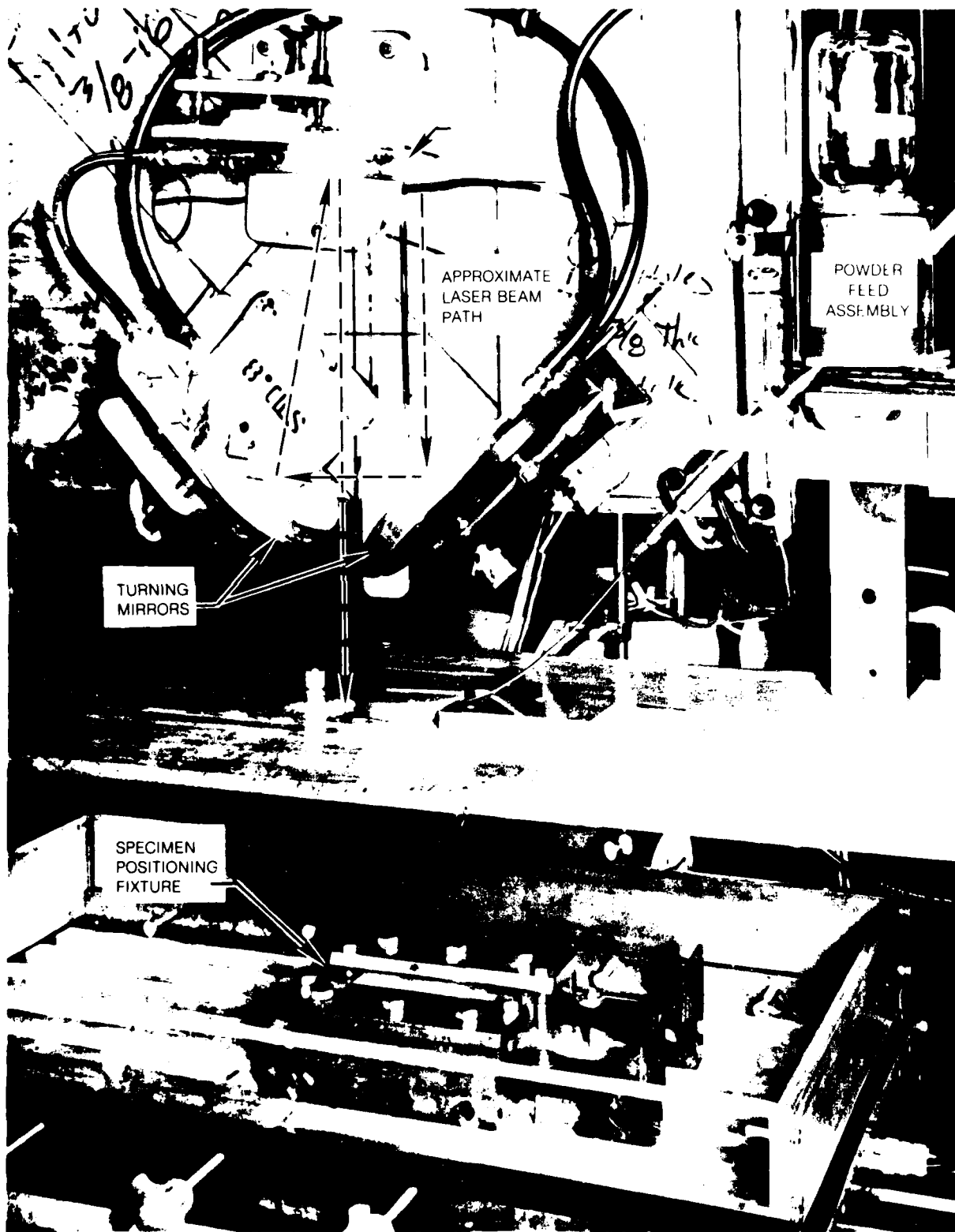
FOCUSING  
MIRROR

TURNING  
MIRROR

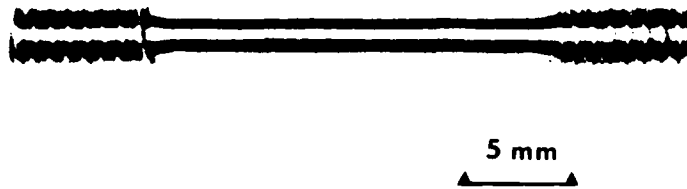
POWDER FEED  
ASSEMBLY

### LAYERGLAZE WORK STATION FOR 2.54 AND 5.08-cm T-6Al-4V PLATE

MACHINING TABLE LOWERED TO SHOW PROTECTIVE ATMOSPHERE CHAMBER AND SPECIMEN POSITIONING FEATURE

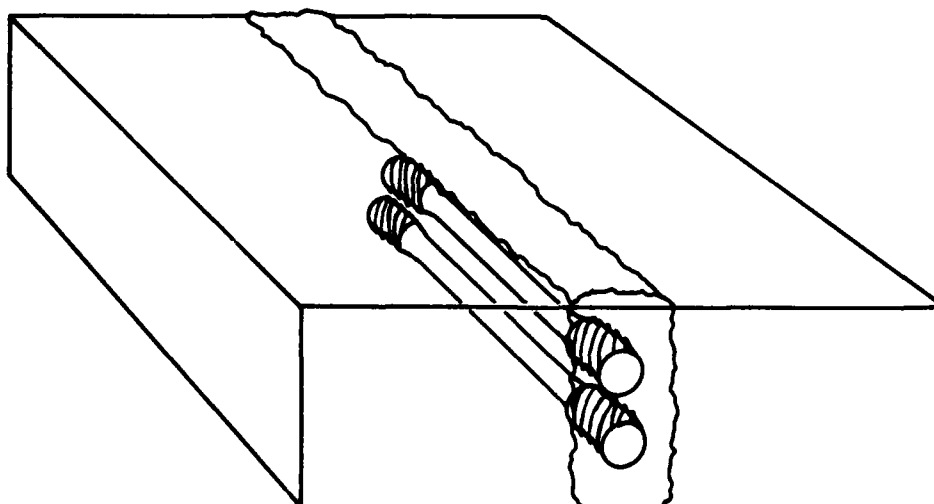


**FUSION ZONE TENSILE SPECIMEN**



**LOCATION OF TENSILE SPECIMENS IN FUSION ZONE  
... WELDS IN FIG. 7**

FIG. 6

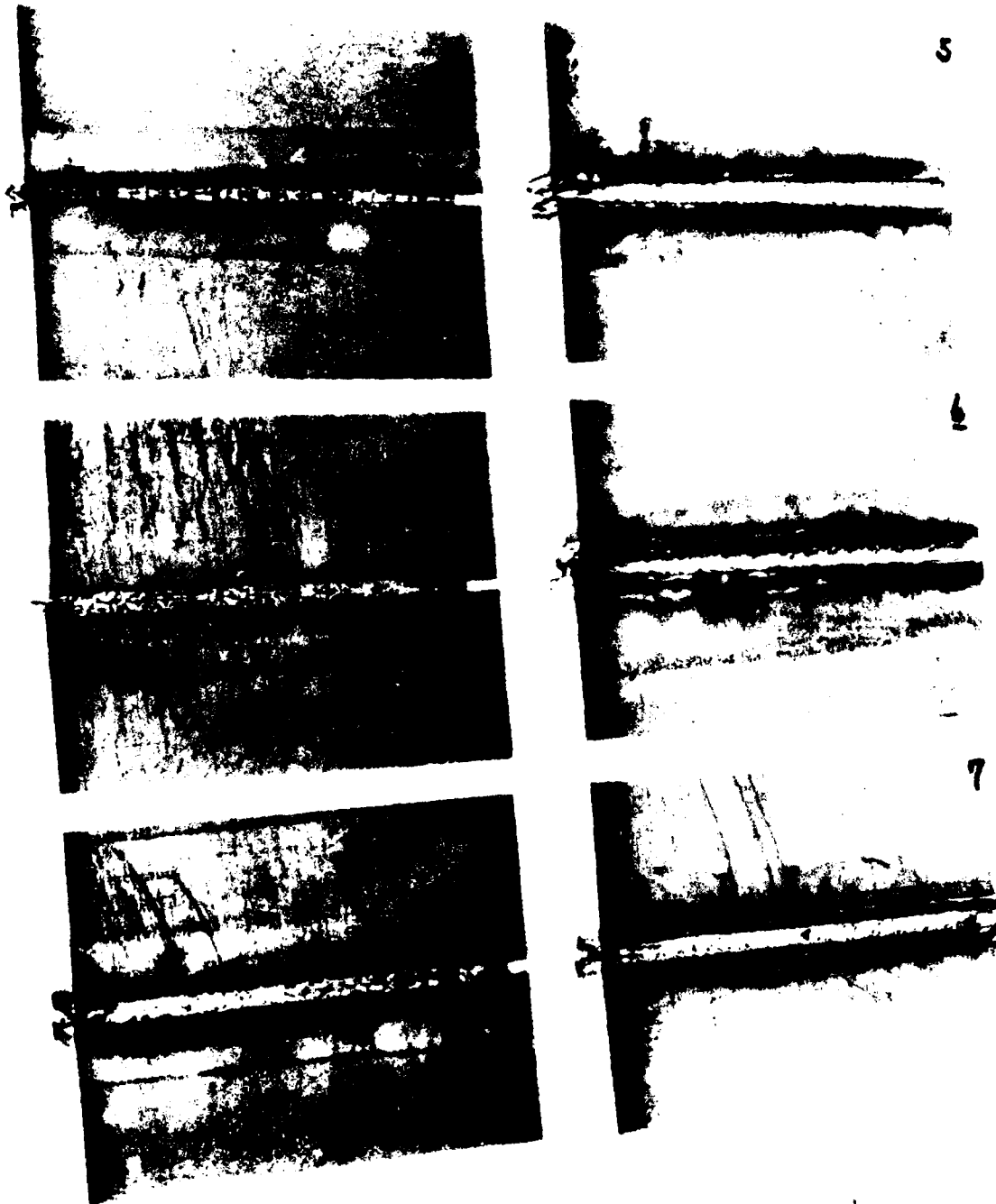


R84-915797-4

FIG. 7

# NARROW-GAP/LAYERGLAZE WELD SPECIMENS

1.27-cm Ti-6Al-4V PLATE WITH BOTTOM GAP CLOSURE



5 cm

84-2-40-3

**UPPER FREE SURFACE, NARROW-GAP/LAYERGLAZE WELDS IN FIG. 7**

Ti-6Al-4V (WT %) POWDER FEEDSTOCK: (1 AND 2) PREALLOYED Ti-6Al-4V, (7) MECHANICALLY BLENDED Ti-6Al-4V



(7)

(2)

(1)

**UPPER FREE SURFACE, NARROW-GAP/LAYERGLAZE WELDS IN FIG. 7**

MECHANICALLY BLENDED POWDER FEEDSTOCK (WT %): SPECIMEN (3) Ti-6Al-4V-1.5Er, SPECIMEN (5) Ti-6Al-4V-1.5Y, SPECIMEN (6) Ti-6Al-4V-3Nd



(3)



(5)



(6)



1 mm

1 mm

### LAYERGLAZE/NARROW-GAP WELD SPECIMEN

5.08-cm Ti-6Al-4V PLATE WITH CENTRAL GAP CLOSURE. PREALLOYED Ti-6Al-4V POWDER FEEDSTOCK



2 cm

MACRO PHOTOGRAPH, SIDE 1



SIDE ONE

SIDE TWO

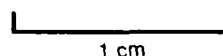
1 cm

WELD CROSS SECTION

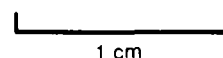
**TOP SURFACES OF FUSION ZONE, 5.08-cm NARROW-GAP/LAYERGLAZE WELD SPECIMEN**



SIDE ONE



SIDE TWO



**5.08-cm LAYERGLAZE/NARROW-GAP WELD SPECIMEN; GRAIN STRUCTURE OF SIDE ONE**



3 mm

**5.08-cm LAYERGLAZE/NARROW-GAP WELD SPECIMEN; GRAIN STRUCTURE OF SIDE TWO**



3 mm

### 1.27-cm LAYERGLAZE/NARROW GAP WELD SPECIMEN NO. 7, FUSION ZONE GRAIN STRUCTURE

(MECHANICALLY-BLENDED Ti-6Al-4V POWDER FEEDSTOCK, NO RARE-EARTH ELEMENT ADDED)



LASER BEAM  
DIRECTION

Q OF  
FUSION ZONE

1mm

**1.27-cm LAYERGLAZE/NARROW GAP WELD SPECIMEN NO. 3, FUSION ZONE GRAIN STRUCTURE**

LASER BEAM  
DIRECTION

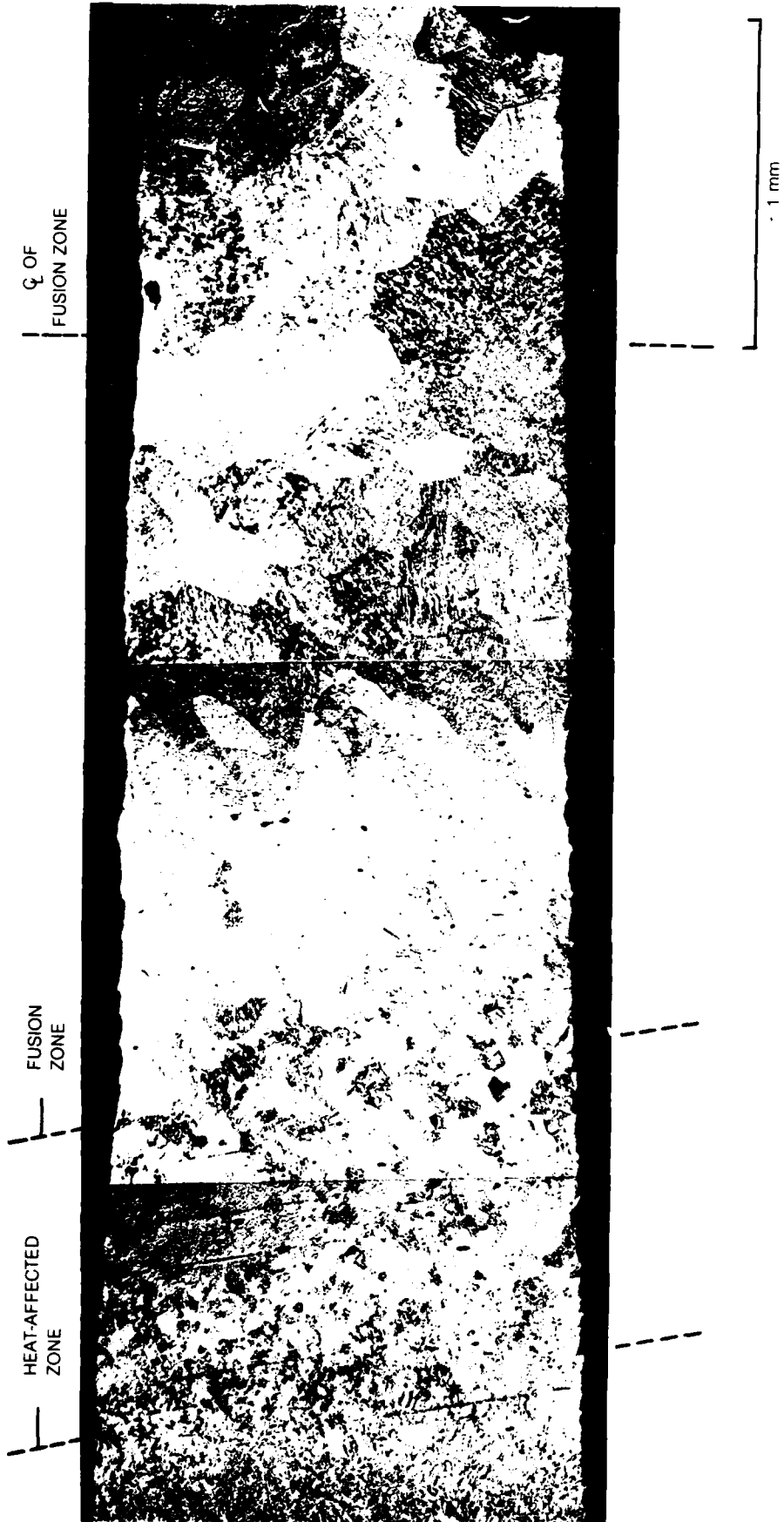
(MECHANICALLY-BLENDED Ti-6Al-4V-1.5 Er POWDER FEEDSTOCK)



Q OF  
FUSION ZONE

1mm

**1.27-cm LAYERGLAZE/NARROW GAP WELD SPECIMEN NO. 3.**  
**VARIATION IN MICROSTRUCTURE ACROSS WELD**  
(MECHANICALLY-BLENDED Ti-6Al-4V-1.5Er POWDER FEEDSTOCK)



**AS-LAYERGLAZED FUSION ZONE MICROSTRUCTURE, SPECIMEN NO. 3**  
(LIGHT MICROGRAPH, ERBIUM OXIDE PARTICLES IN  $\alpha'$ -HCP MARTENSITE)



# 1.27-cm LAYERGLAZE/NARROW GAP WELD SPECIMEN NO. 5, FUSION ZONE GRAIN STRUCTURE

(MECHANICALLY-BLENDED Ti-6Al-4V-1.5Y POWDER FEEDSTOCK)



**AS-LAYERGLAZED FUSION ZONE MICROSTRUCTURE, SPECIMEN NO. 5**  
(LIGHT MICROGRAPH, YTTRIUM OXIDE PARTICLES IN  $\alpha'$  HCP MARTENSITE)



10 $\mu$ m

**1.27-cm LAYERGLAZE/NARROW GAP WELD SPECIMEN NO. 6, FUSION ZONE GRAIN STRUCTURE**

(MECHANICALLY-BLENDED Ti-6Al-4V-3Nd POWDER FEEDSTOCK)



LASER BEAM  
DIRECTION

Q OF  
FUSION ZONE

1mm

**AS-LAYERGLAZED FUSION ZONE MICROSTRUCTURE, SPECIMEN NO. 6**

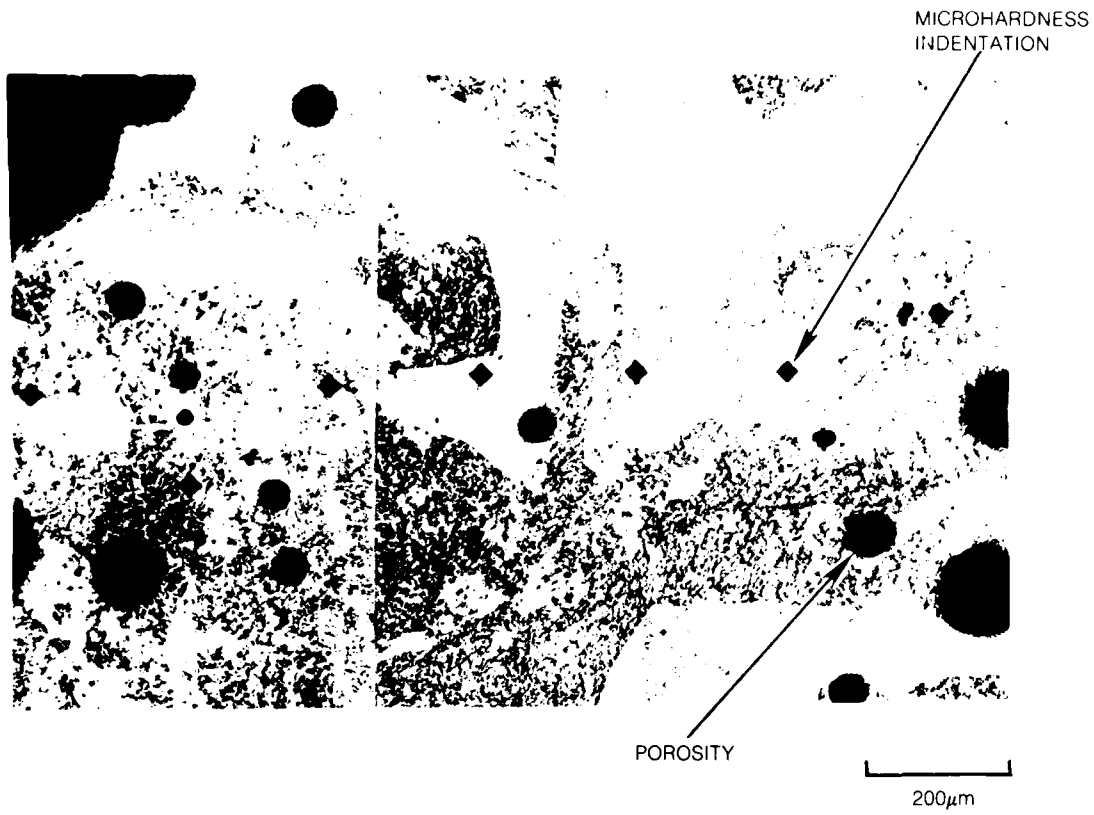
(LIGHT MICROGRAPH, NEODYMIUM OXIDE IN  $\alpha'$  HCP MARTENSITE)



10 $\mu$ m

### FUSION ZONE GRAIN STRUCTURE

SPECIMEN AS-LAYERGLAZED FROM MECHANICALLY-BLENDED Ti-6Al-2Sn-4Zr-6Mo-1Er POWDER FEEDSTOCK



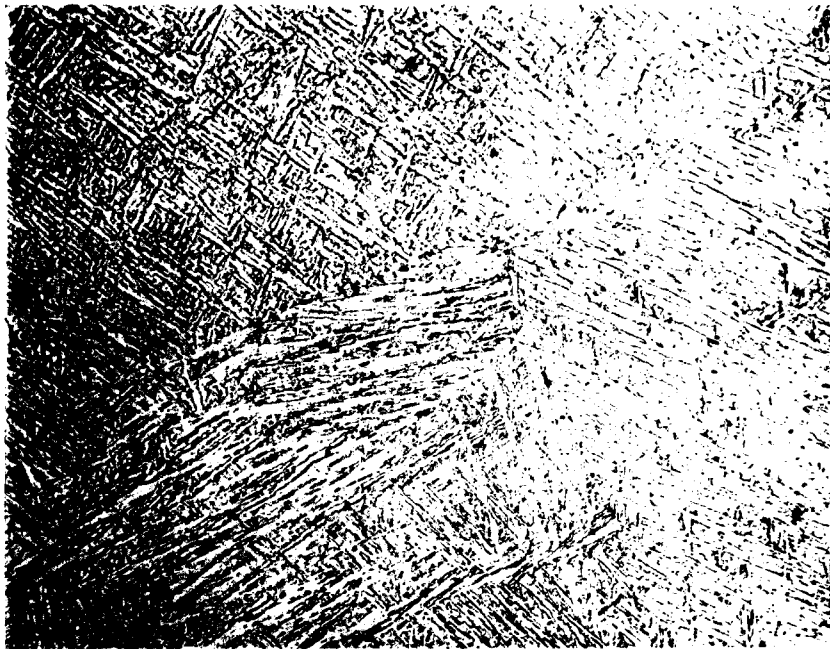
**FUSION ZONE MICROSTRUCTURE, SPECIMEN  
AS-LAYERGLAZED FROM Ti-6242-1 Er POWDER**

( $\alpha'$  HCP MARTENSITE; MOST ERBIUM OXIDE PARTICLES TOO SMALL TO BE VISIBLE)



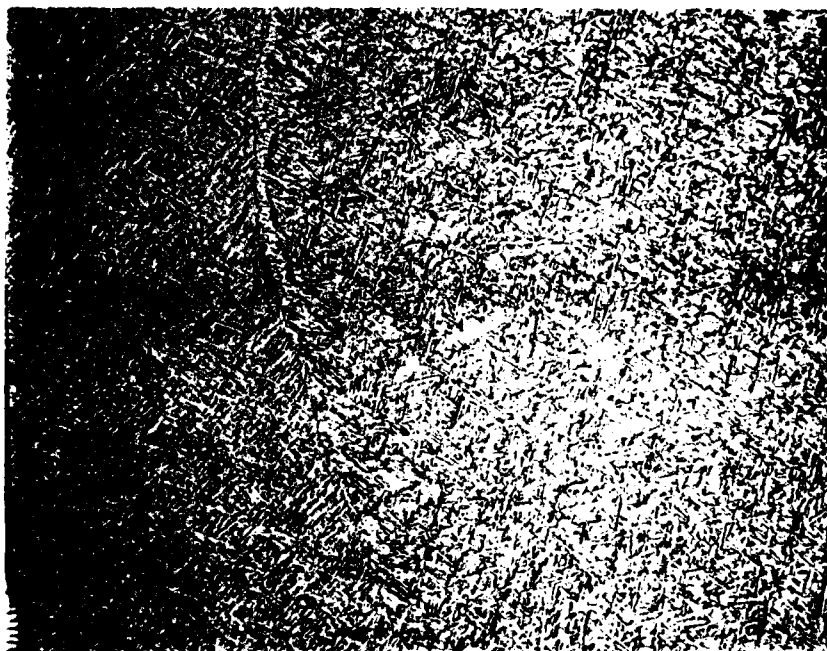
### AGED FUSION ZONE MICROSTRUCTURES

(SPECIMENS LAYERGLAZED AND ANNEALED AT 800°C (1472°F) FOR 75 min)



MECHANICALLY-BLENDED Ti-6Al-4V  
POWDER FEEDSTOCK

20µm



MECHANICALLY BLENDED Ti-6Al-4V-3Nd  
POWDER FEEDSTOCK

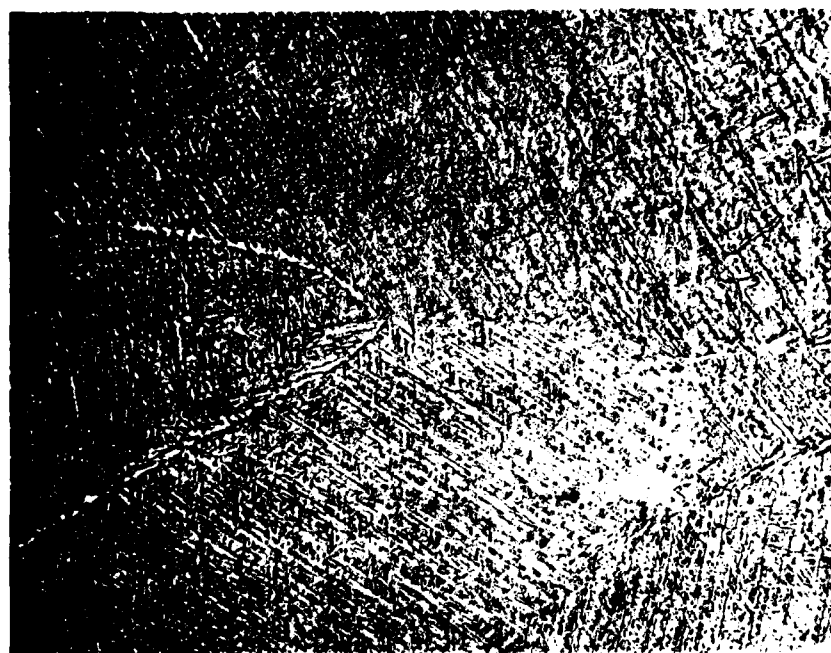
20µm

**AGED FUSION ZONE MICROSTRUCTURES**

(SPECIMENS LAYERGLAZED AND ANNEALED AT 800°C (1472°F) FOR 75 min)



MECHANICALLY-BLENDED Ti-6Al-4V-1.5Y FEEDSTOCK

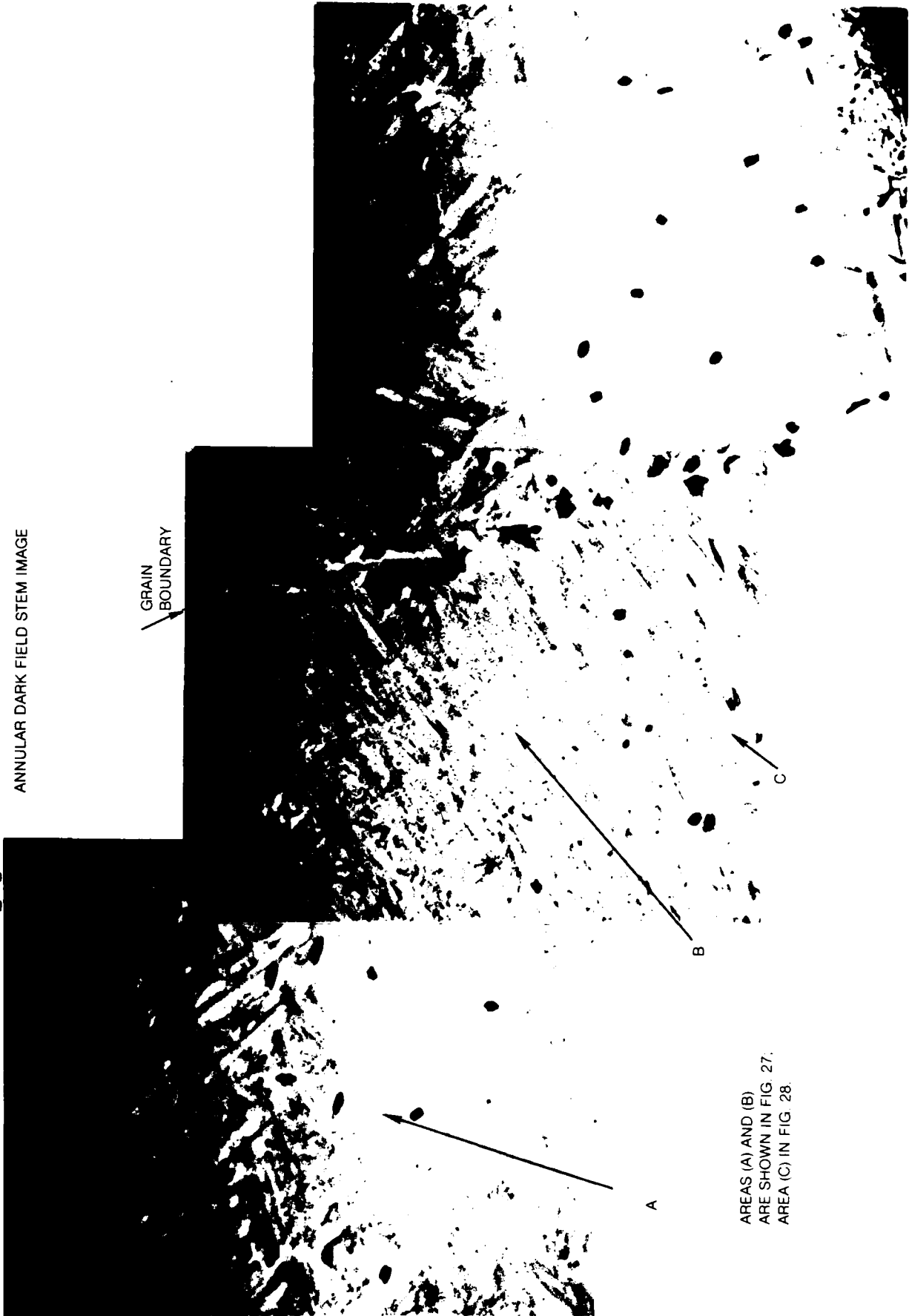


MECHANICALLY-BLENDED Ti-6Al-4V-1.5Er FEEDSTOCK

20μm

**DISTRIBUTION OF  $Er_2O_3$  IN SPECIMEN AS-LAYERGLAZED FROM Ti-6Al-4V-1.5Er POWDER**

ANNULAR DARK FIELD STEM IMAGE



GRAIN  
BOUNDARY

A

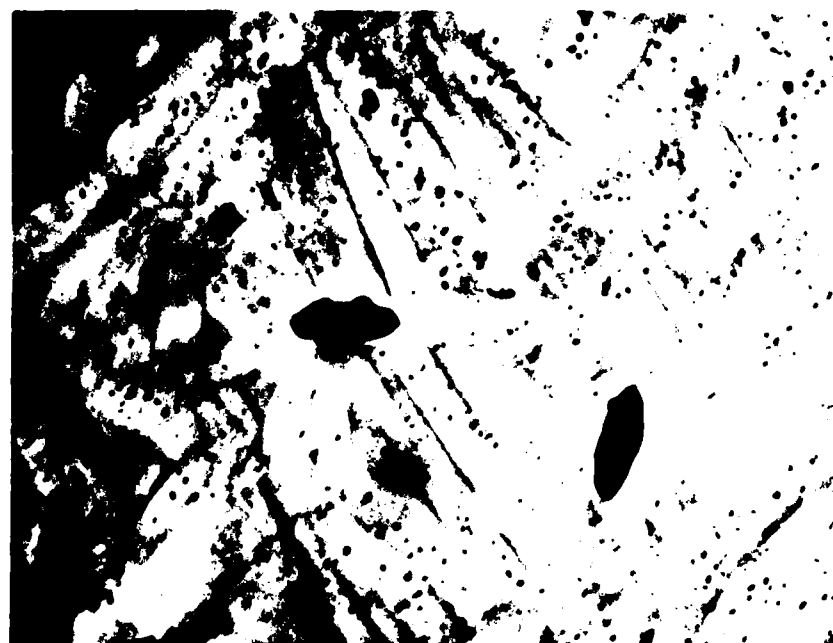
B

C

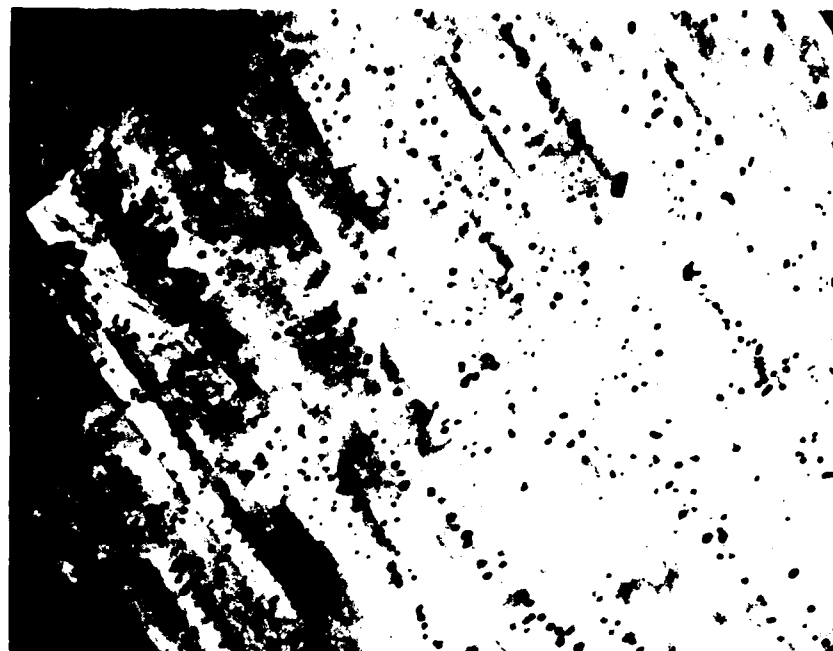
AREAS (A) AND (B)  
ARE SHOWN IN FIG. 27.  
AREA (C) IN FIG. 28.

**BIMODAL SIZE DISTRIBUTION OF  $\text{Er}_2\text{O}_3$  IN SPECIMEN AS-LAYERGLAZED  
FROM Ti-6Al-4V-1.5Er**

MEAN SIZES OF 280 AND 40 nm  
ANNULAR DARK FIELD STEM IMAGES



AREA (A) IN FIG. 26

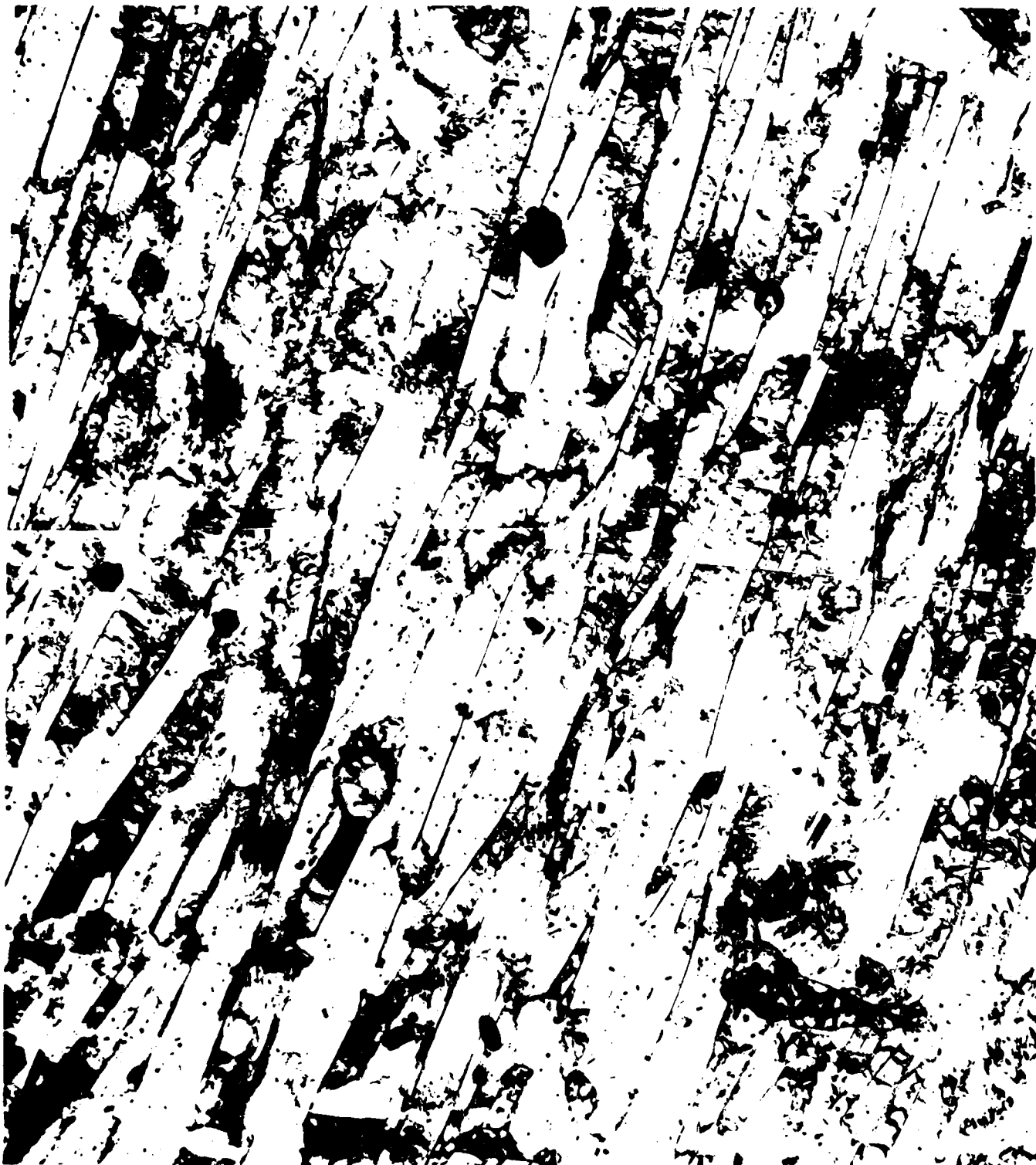


AREA (B) IN FIG. 26

400 nm

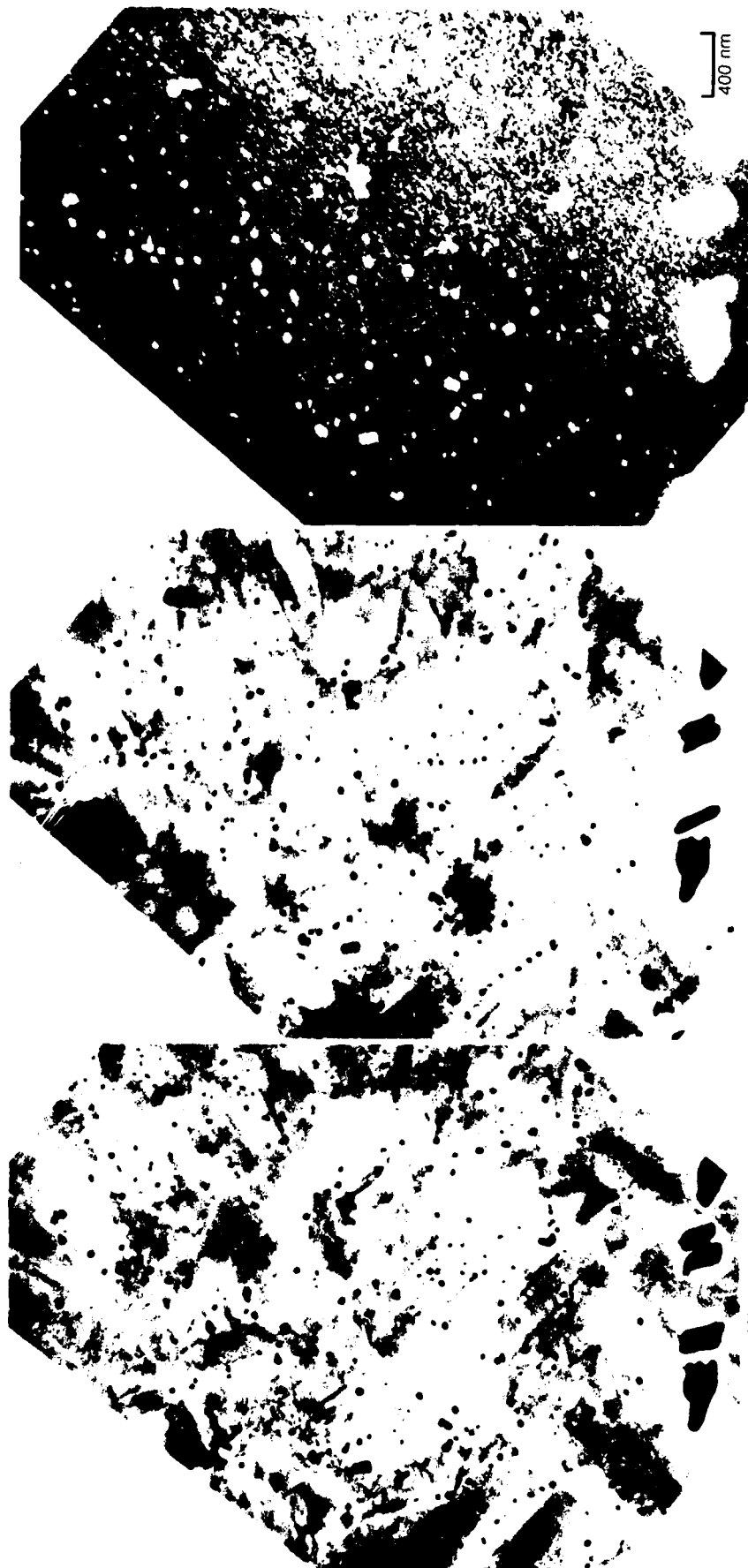
**BIMODAL SIZE DISTRIBUTION OF  $\text{Er}_2\text{O}_3$  IN SPECIMEN AS-LAYERGLAZED  
FROM Ti-6Al-4V-1.5Er POWDER**

AREA (C) IN FIG. 26  
BRIGHT FIELD CTEM IMAGE



1  $\mu\text{m}$

**Er<sub>2</sub>O<sub>3</sub> DISTRIBUTION IN SPECIMEN AS-LAYERGLAZED FROM TI-6AL-4V-1.5Er POWDER**



(A) ANNULAR DARK FIELD STEM STEREO IMAGE

(B) BACKSCATTERED ELECTRON IMAGE,  
AREA OF (A)

# STEM IMAGE AND ENERGY DISPERSIVE X-RAY SPECTRUM, $\text{Er}_2\text{O}_3$ IN SPECIMEN AS-LAYERGLAZED FROM TI-6AL-4V-1.5ER POWDER

120 kV; 5 nm BEAM SIZE; Al  $K\alpha$  AND Er  $M\alpha$  PEAKS OVERLAP

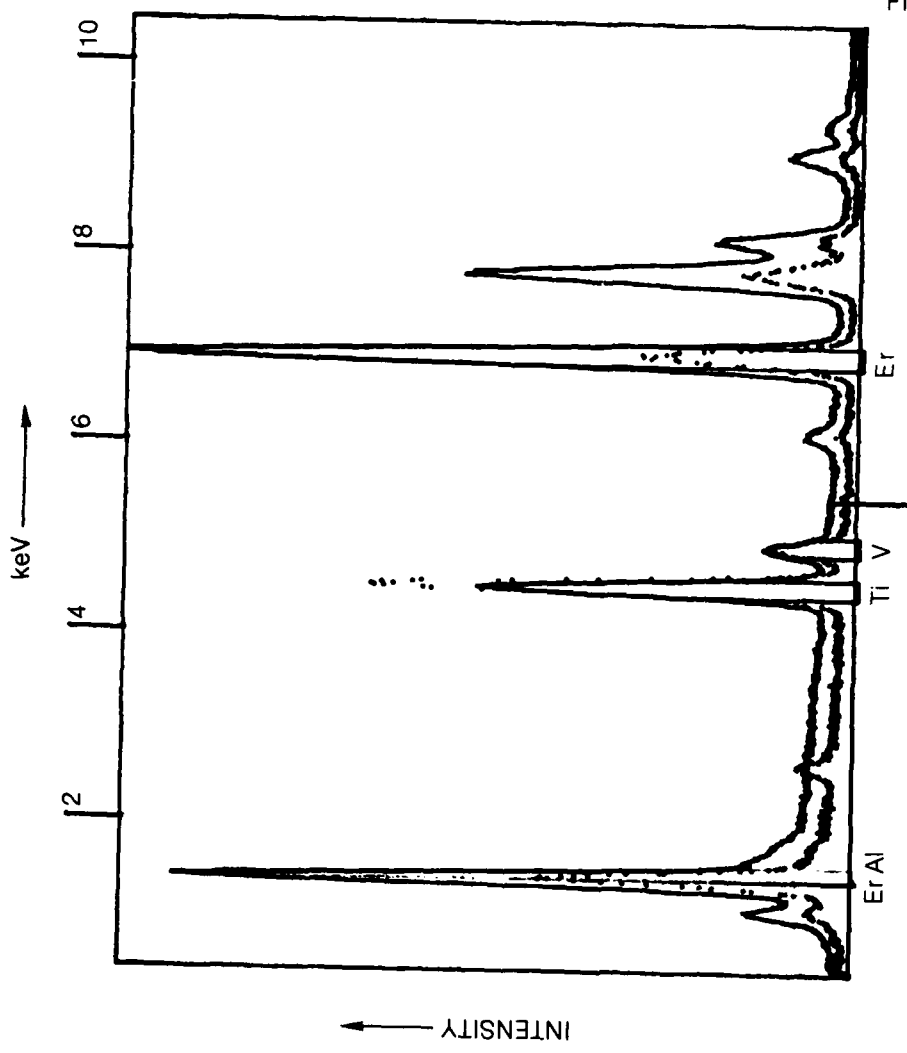
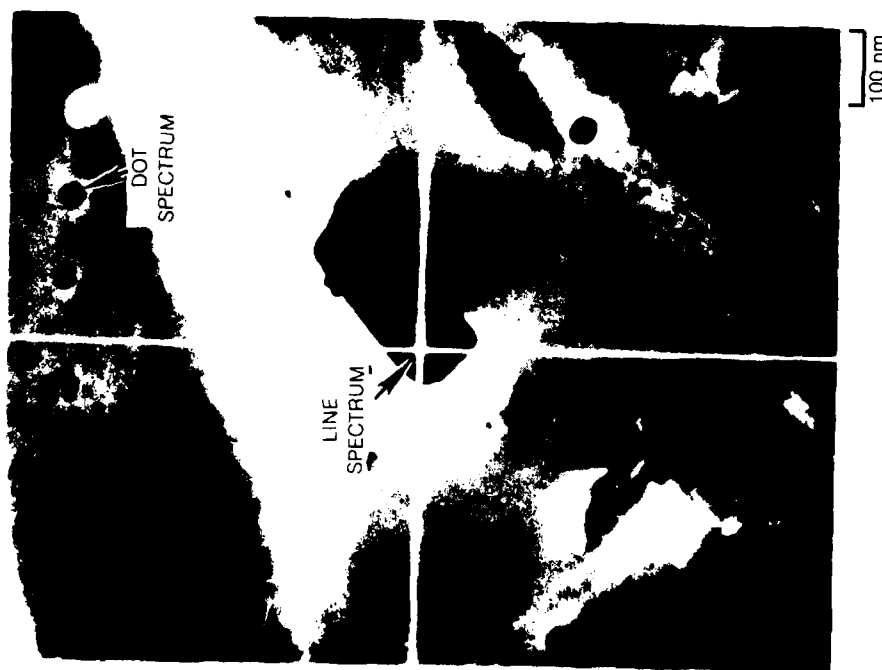


FIG. 30

**INTERDENDRITIC  $\text{Er}_2\text{O}_3$  IN SPECIMEN AS-LAYERGLAZED<sup>SM</sup> FROM Ti-6Al-4V-1.5Er POWDER**

(A) DARK FIELD CTEM,  $g = 400$  (B) SELECTED AREA DIFFRACTION PATTERN FROM (A), [001] ZONE AXIS. POINTER MARKS 400  
(C) AND (D) [001] ZONE AXIS CONVERGENT BEAM DIFFRACTION PATTERNS FROM (A), 40 nm BEAM SIZE



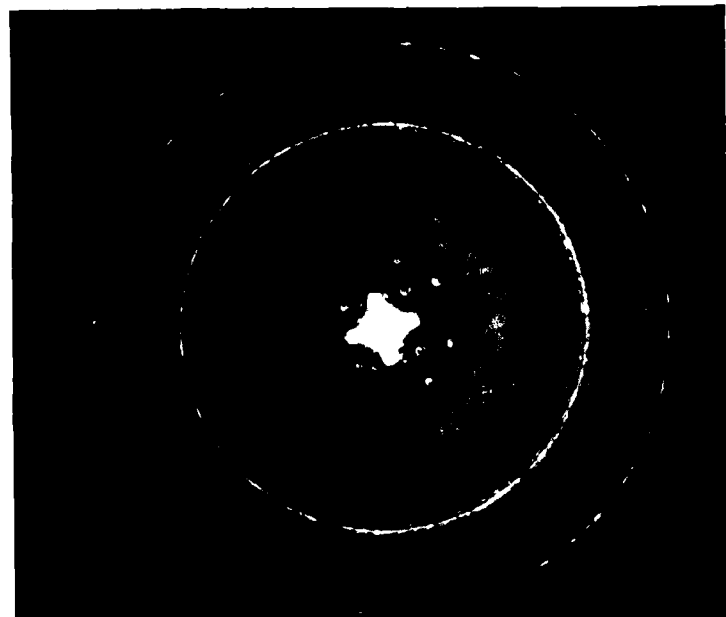
(A)



(B)



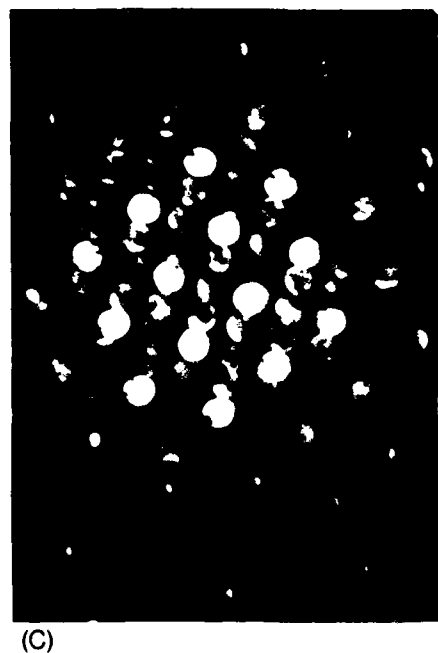
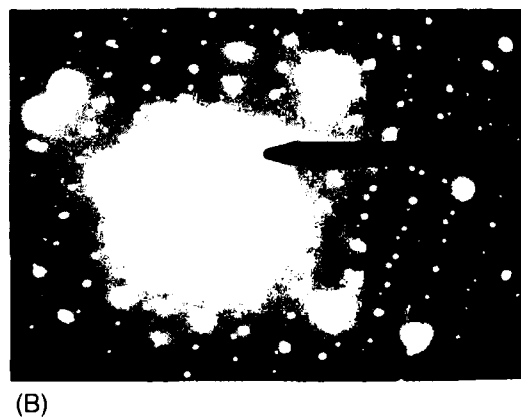
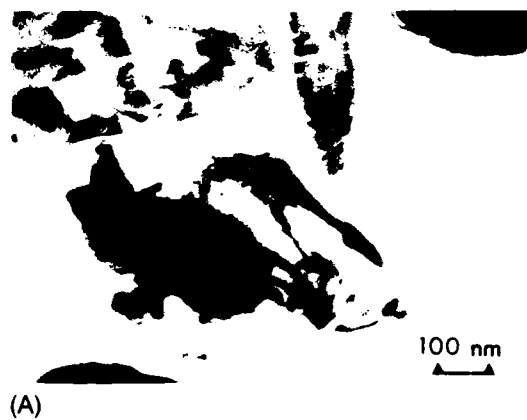
(C)



(D)

**INTERDENDRITIC  $\text{Er}_2\text{O}_3$  IN SPECIMEN AS-LAYERGLAZED FROM Ti-6Al-4V-1.5Er POWDER**

(A) DARK FIELD CTEM,  $g = 2\bar{2}\bar{2}$ . (B) SELECTED AREA DIFFRACTION PATTERN FROM (A), [011] ZONE AXIS. POINTER MARKS  $2\bar{2}\bar{2}$   
(C) AND (D) [011] ZONE AXIS CONVERGENT BEAM DIFFRACTION PATTERNS FROM (A), 40 nm BEAM SIZE

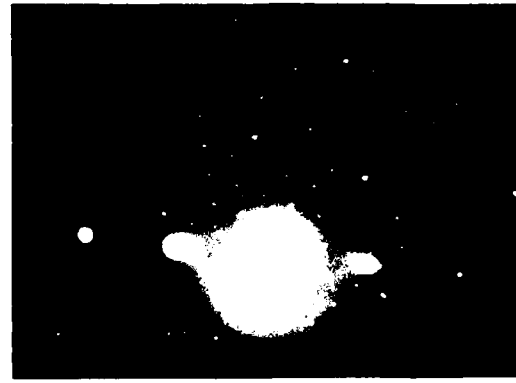


**INTERDENDRITIC  $\text{Er}_2\text{O}_3$  IN SPECIMEN AS-LAYERGLAZED FROM Ti-6Al-4V-1.5Er POWDER**

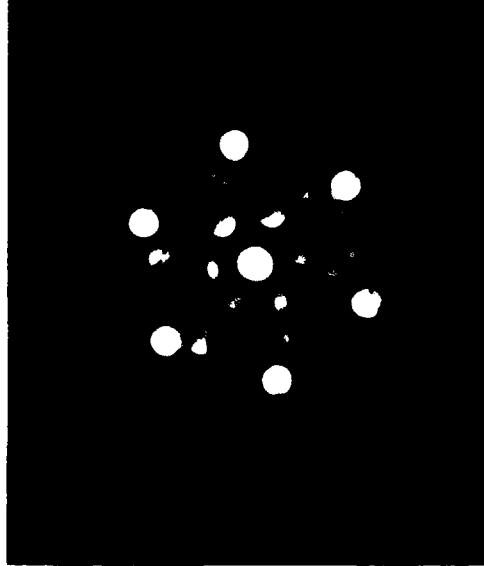
(A) DARK FIELD CTEM,  $g = 440$ . (B) SELECTED AREA DIFFRACTION PATTERN FROM (A),  $[\bar{1}11]$  ZONE AXIS. POINTER MARKS 440  
(C) AND (D)  $[\bar{1}11]$  ZONE AXIS CONVERGENT BEAM DIFFRACTION PATTERNS FROM (A). 40 nm SPOT SIZE



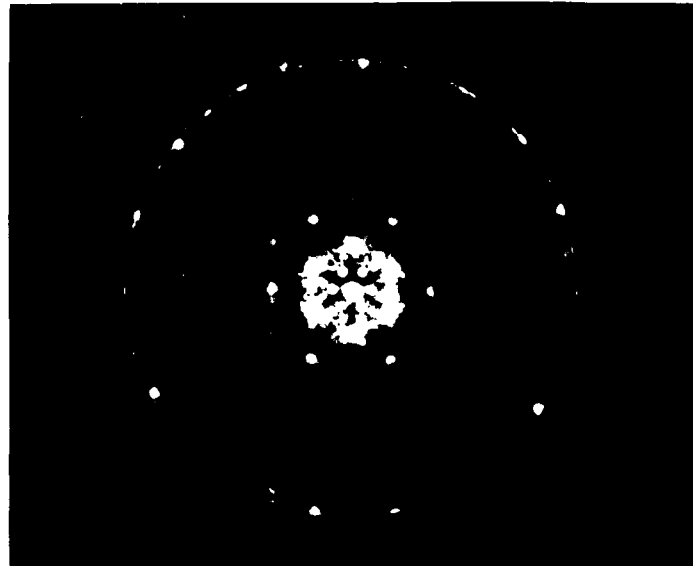
(A)



(B)



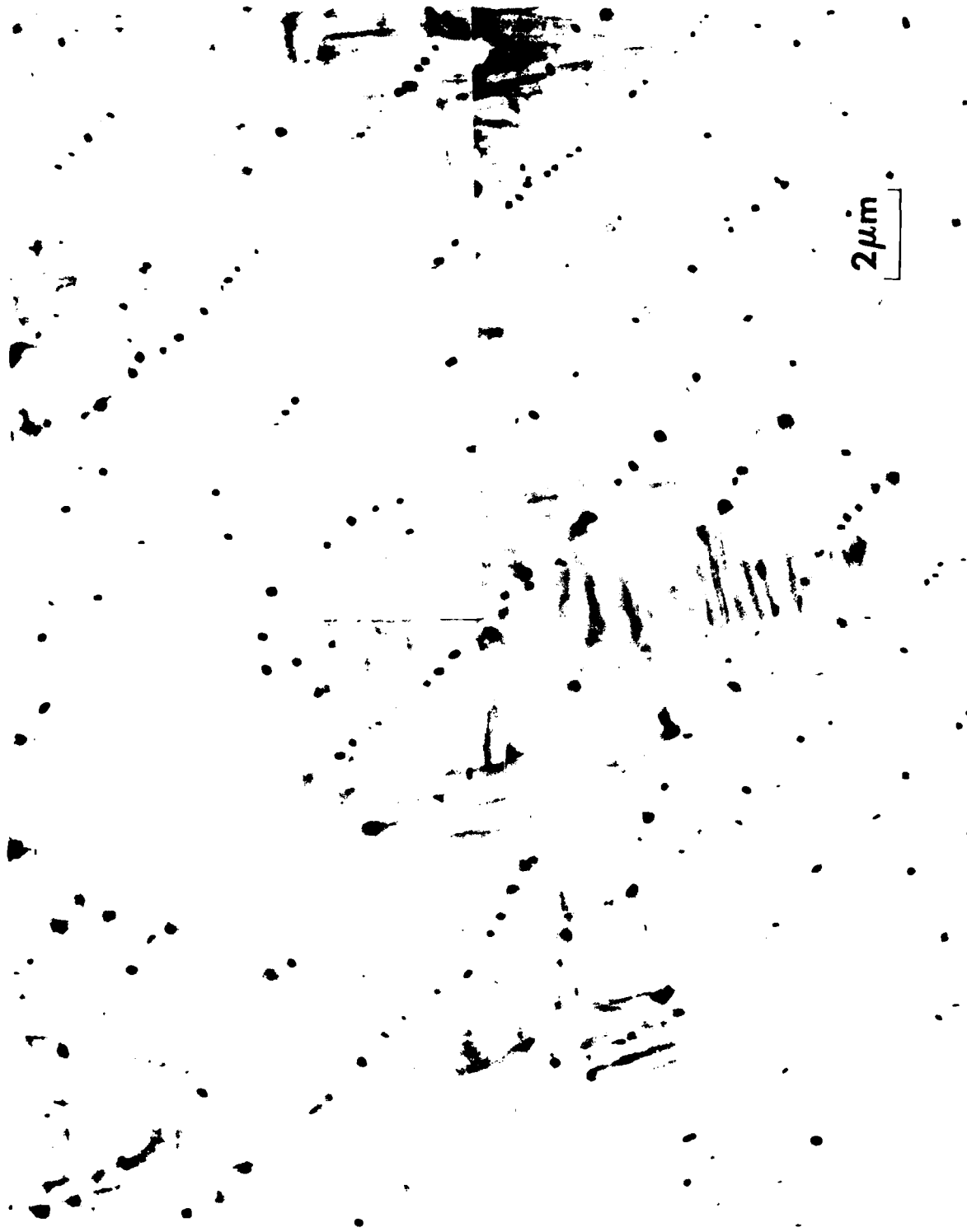
(C)



(D)

**DISTRIBUTION OF  $Y_2O_3$  IN SPECIMEN AS-LAYERGLAZED FROM TI-6AL-4V-1.5Y**

PREDOMINATELY INTERDENDRITIC  $Y_2O_3$  PRECIPITATION  
ANNULAR DARK FIELD STEM IMAGE



2  $\mu\text{m}$

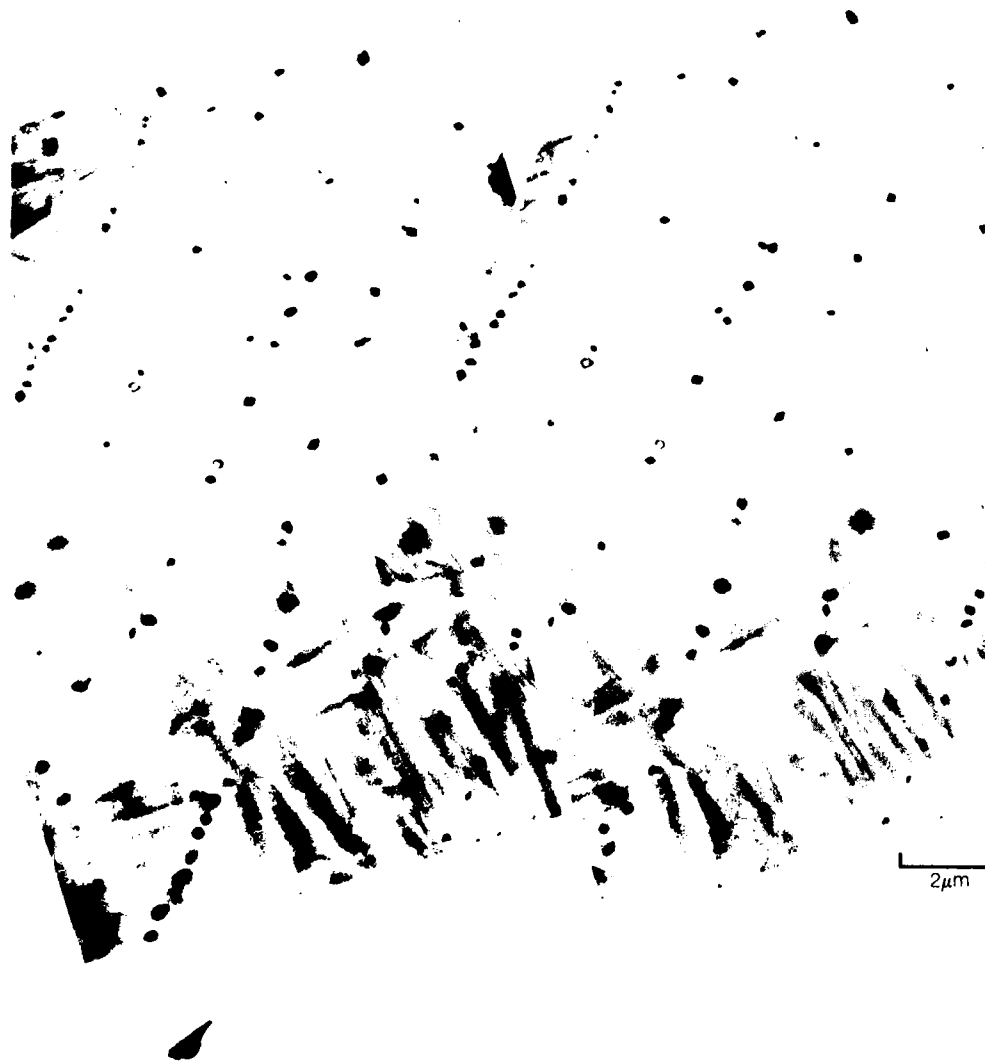
**DISTRIBUTION OF  $Y_2O_3$  IN SPECIMEN AS-LAYERGLAZED FROM TI-6Al-4V-1.5Y POWDER**

BRIGHT FIELD CTEM  
AREA AT LOWER RIGHT OF FIG. 34. MIRROR IMAGE



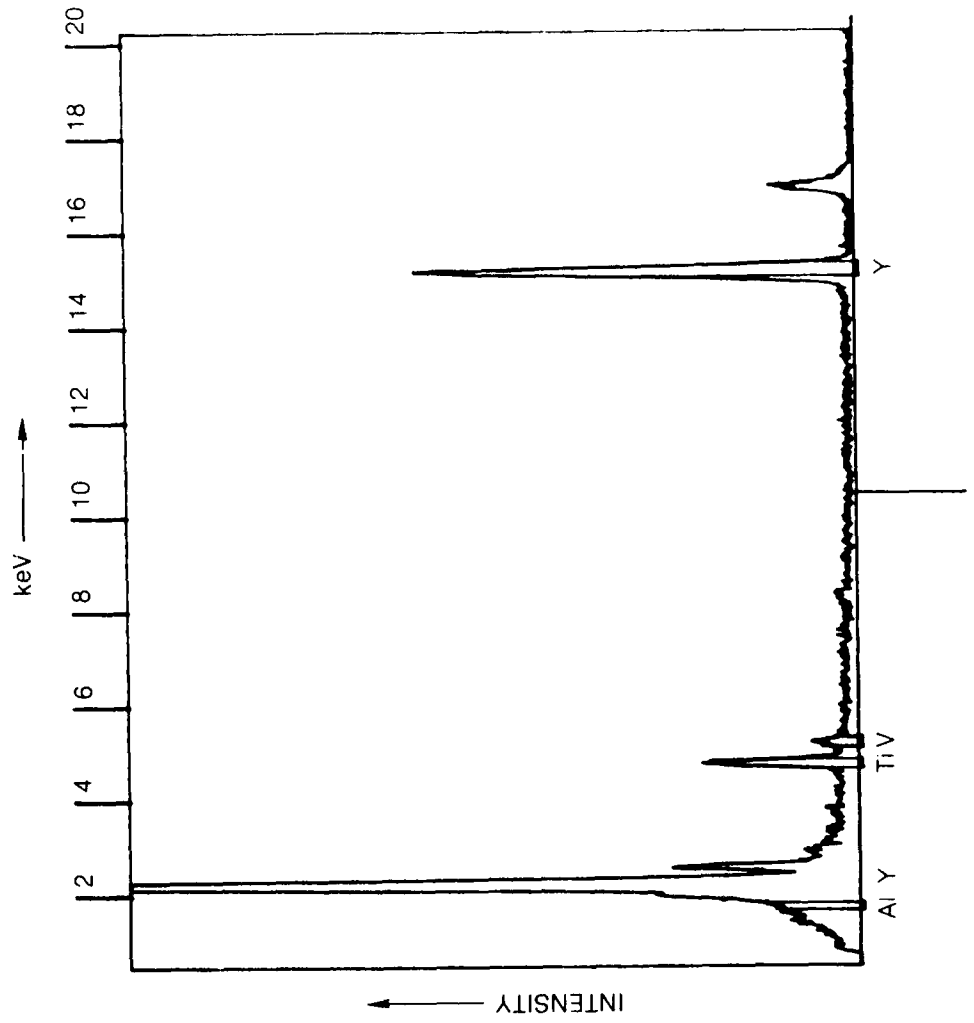
**Y<sub>2</sub>O<sub>3</sub> DISTRIBUTION IN SPECIMEN AS-LAYERGLAZED FROM Ti-6Al-4V-1.5Y POWDER**

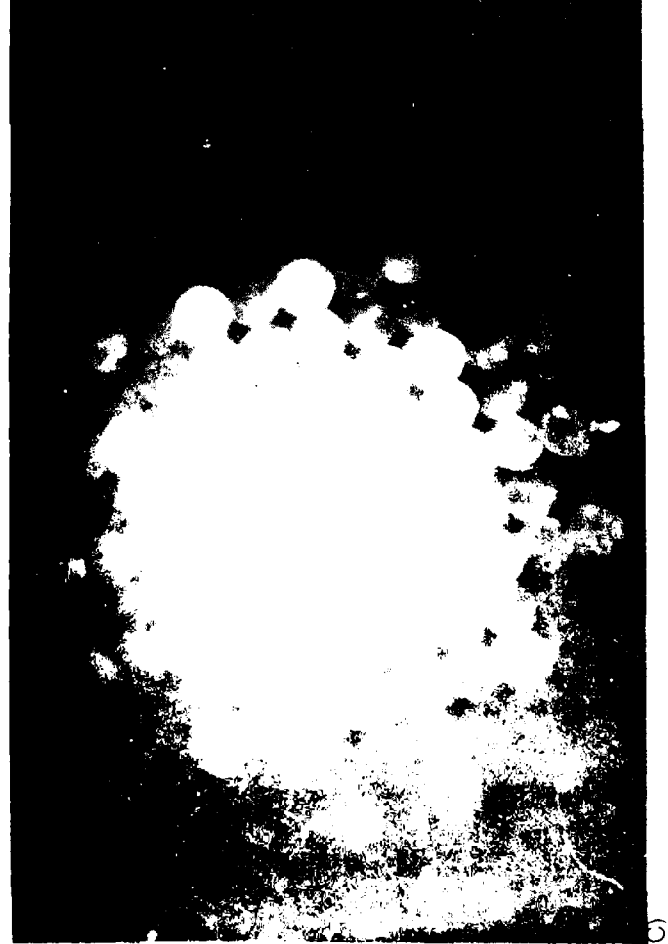
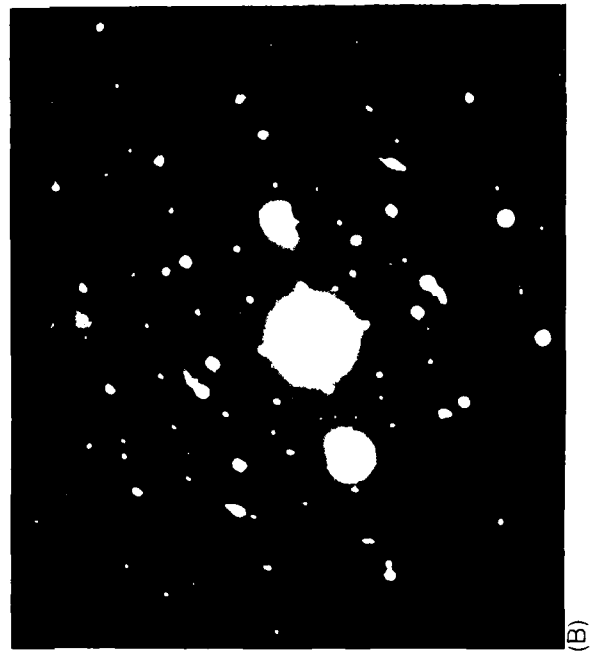
ANNULAR DARK FIELD STEM STEREO IMAGE  
AREA IN LOWER RIGHT, FIG. 34. ROTATED 90°



**STEM IMAGE AND ENERGY DISPERSIVE X-RAY SPECTRUM,  $Y_2O_3$  IN SPECIMEN  
AS-LAYERGLAZED FROM TI-6AL-4V-1.5Y POWDER**

120 kV, 5 nm BEAM SIZE



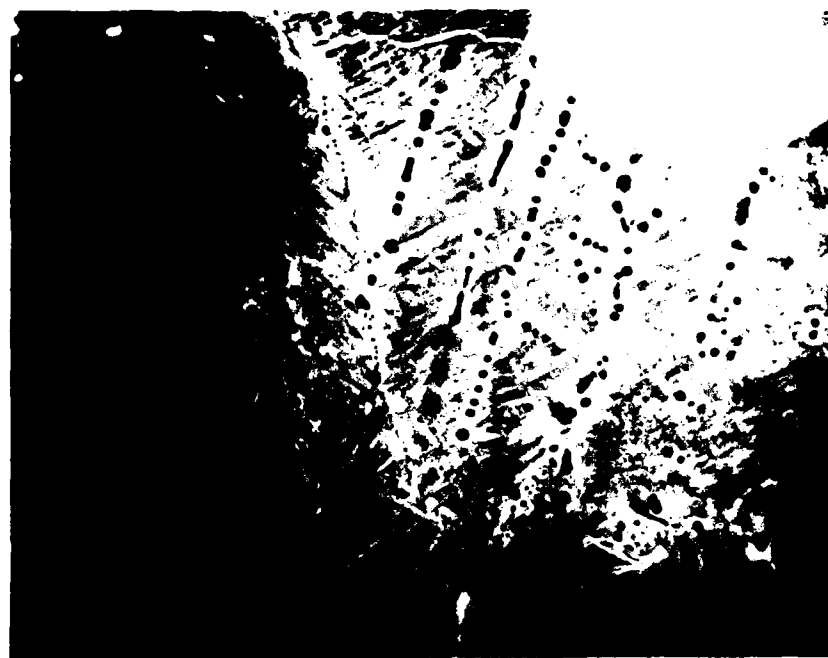


**INTERDENDRITIC  $Y_2O_3$  IN SPECIMEN AS-LAYERGLAZED  
FROM TI-6AL-4V-1.5Y POWDER**

(A) DARK FIELD CTEM,  $g = 400$ . (B) SELECTED AREA DIFFRACTION PATTERN FROM (A), [001] ZONE AXIS, POINTER MARKS 400. (C) [001] ZONE AXIS CONVERGENT BEAM DIFFRACTION PATTERN FROM (A), 40 nm BEAM SIZE

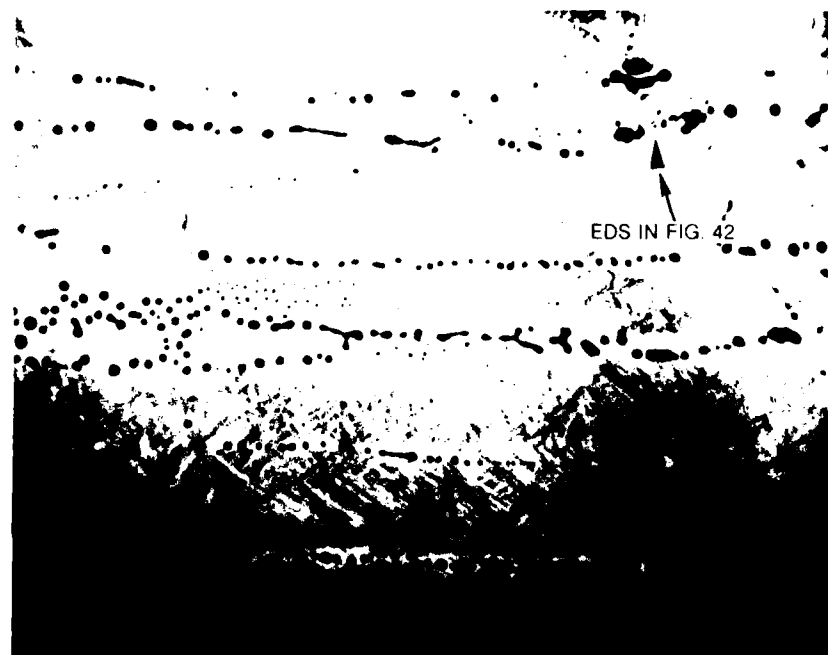
**DISTRIBUTION OF  $\text{Nd}_2\text{O}_3$  IN SPECIMEN  
AS-LAYERGLAZED FROM Ti-6Al-4V-3Nd POWDER**

PREDOMINATELY INTERDENDRITIC  $\text{Nd}_2\text{O}_3$  PRECIPITATION  
ANNULAR DARK FIELD STEM IMAGES



GRAIN  
BOUNDARY

5 $\mu\text{m}$



5 $\mu\text{m}$

**DISTRIBUTION OF  $\text{Nd}_2\text{O}_3$  IN SPECIMEN  
AS-LAYERGLAZED FROM TI-6AL-4V-3ND POWDER**

BRIGHT FIELD CTEM

MIRROR IMAGE OF AREA IN UPPER PHOTOMICROGRAPH, FIG. 39



FIG. 40

5 $\mu\text{m}$

**DISTRIBUTION OF  $Nd_2O_3$  IN SPECIMEN AS-LAYERGLAZED FROM Ti-6Al-4V-3Nd POWDER**

BRIGHT FIELD CTEM. AREA IN RIGHT OF FIG. 40

GRAIN BOUNDARY



GRAIN BOUNDARY

1 μm

**ANNULAR DARK FIELD STEM IMAGE AND ENERGY DISPERSIVE X-RAY SPECTRUM,  
Nd<sub>2</sub>O<sub>3</sub> IN SPECIMEN AS-LAYERGLAGED FROM Ti-6Al-4V-3Nd**

LOCATION OF Nd<sub>2</sub>O<sub>3</sub> SHOWN BY ARROW IN LOWER PHOTOMICROGRAPH OF FIG. 39.

120KV, 5nm BEAM SIZE

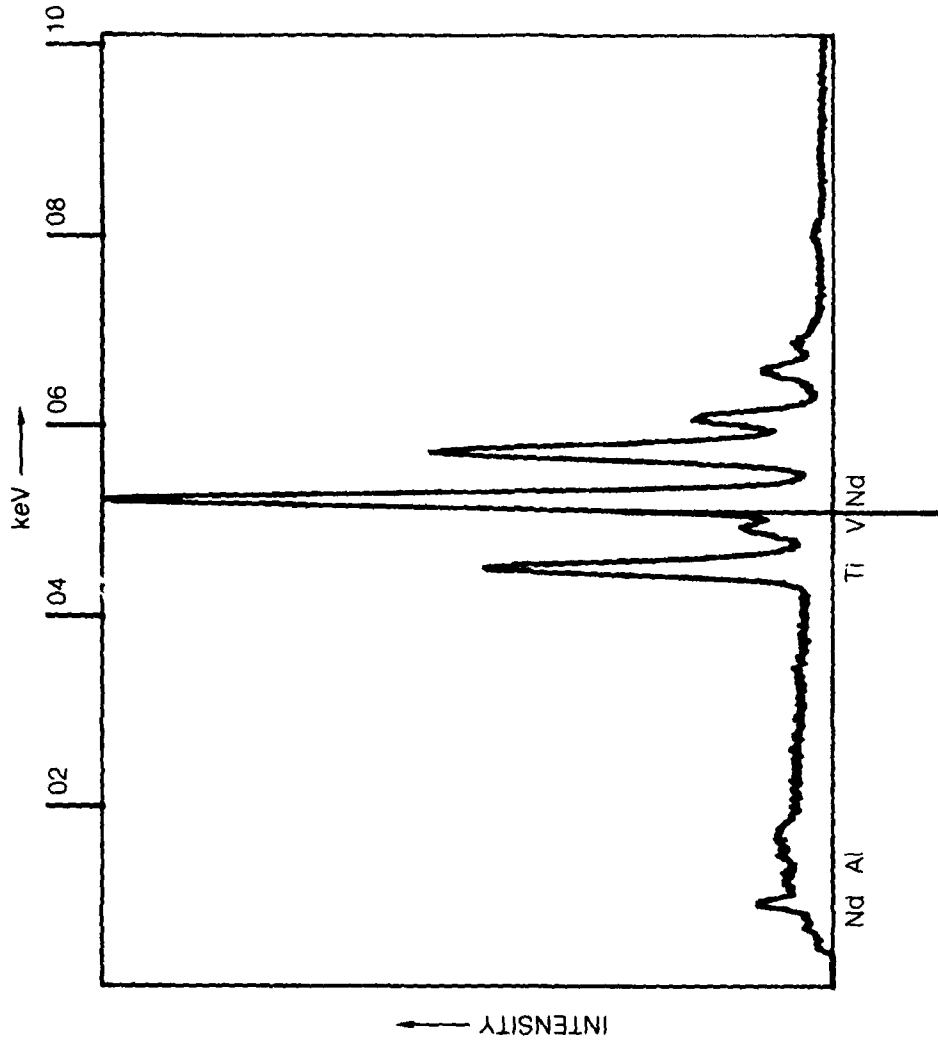
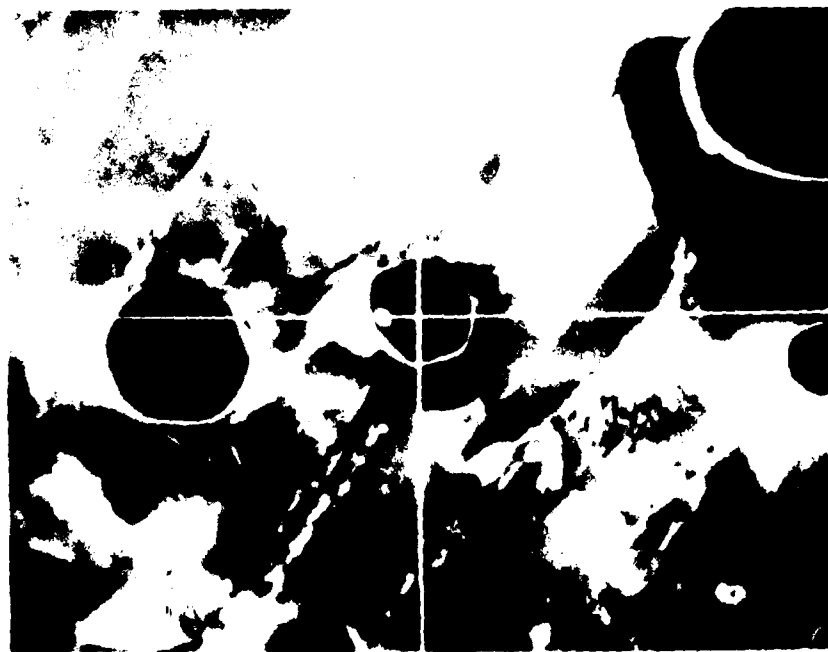


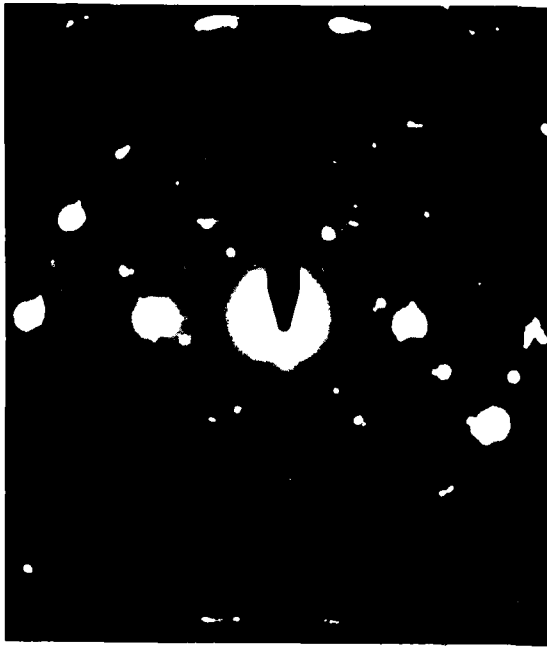
FIG. 42

**INTERDENDRITIC  $\text{Nd}_2\text{O}_3$  IN SPECIMEN AS-LAYERGLAZED FROM Ti-6Al-4V-3Nd POWDER**

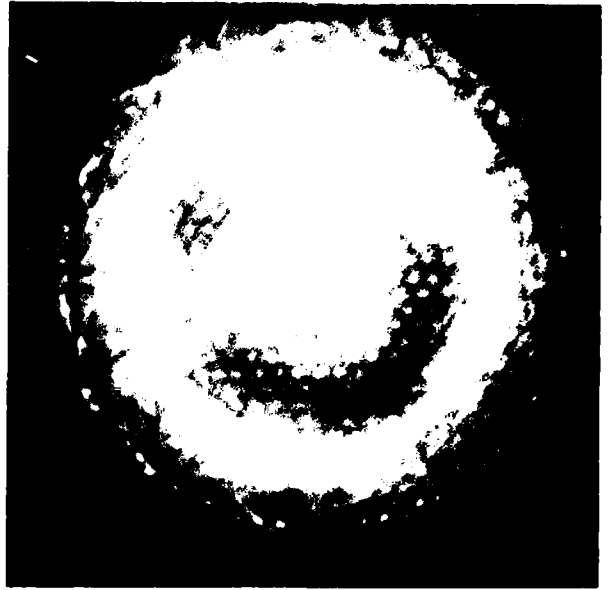
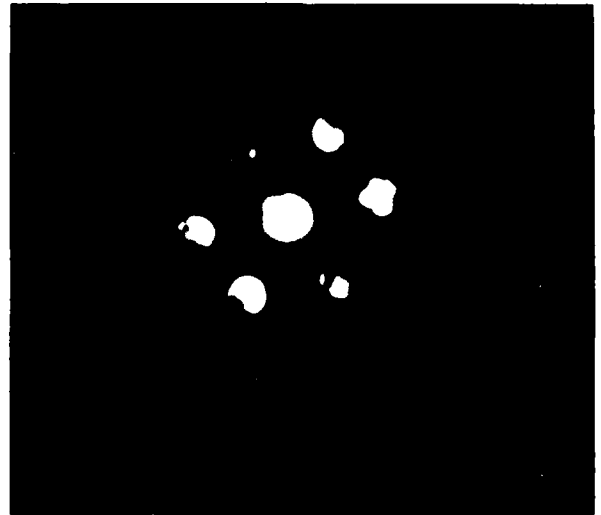
(A) BRIGHT FIELD CTEM. PARTICLE SHOWN IN FIG. 42 (B) SELECTED AREA DIFFRACTION PATTERN FROM (A).  $[\bar{1}\bar{2}\bar{1}3]$  ZONE AXIS. POINTER COVERS 0000. (C) AND (D)  $[\bar{1}\bar{2}\bar{1}3]$  ZONE AXIS CONVERGENT BEAM DIFFRACTION PATTERNS FROM PARTICLE IN (A). 40mm BEAM SIZE.



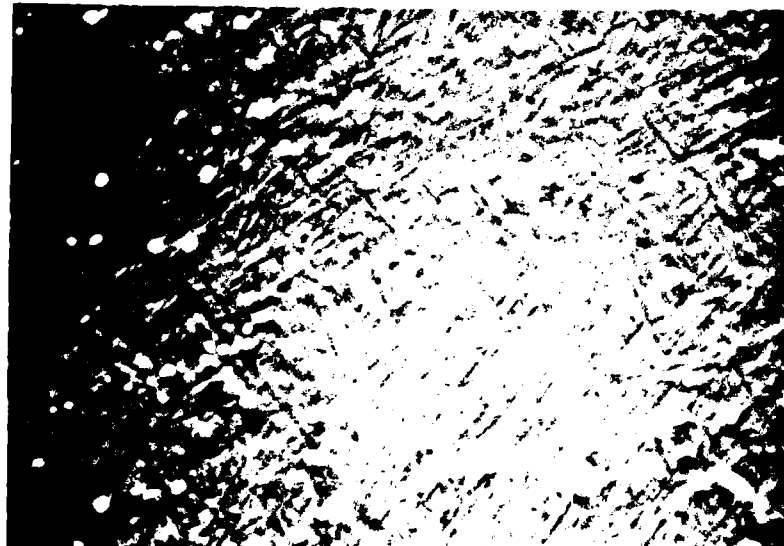
(A)



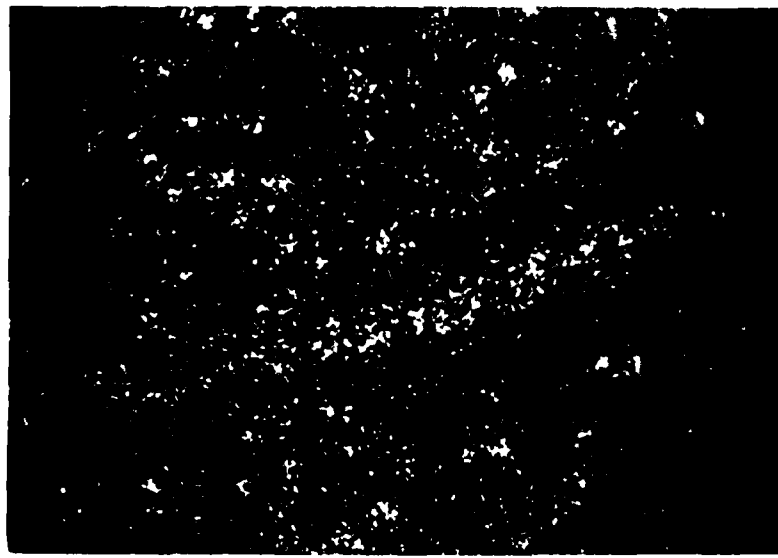
(B)



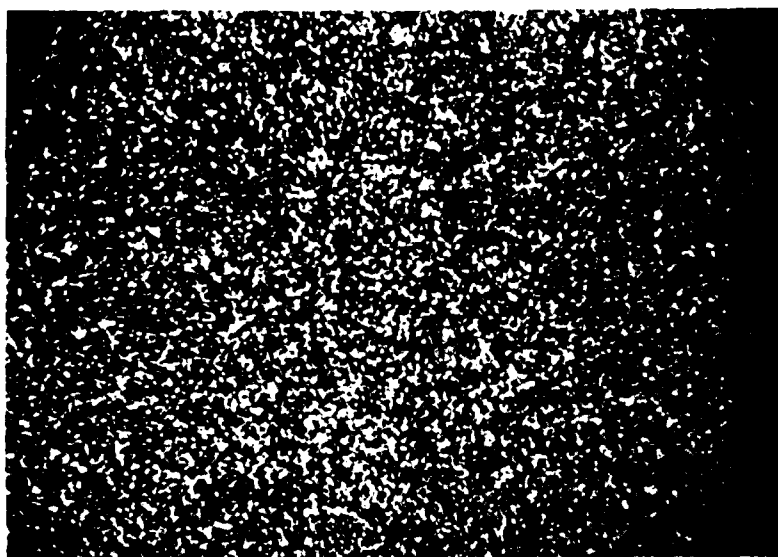
ELECTRON MICROPROBE IMAGES OF SPECIMEN AS-LAYERGLAZED FROM Ti-6Al-2Sn-4Zr-6Mo-1Er



(A) BACKSCATTERED ELECTRON IMAGE.  
ARROWS SHOW  $Er_2O_3$  PRECIPITATION  
AT GRAIN BOUNDARY



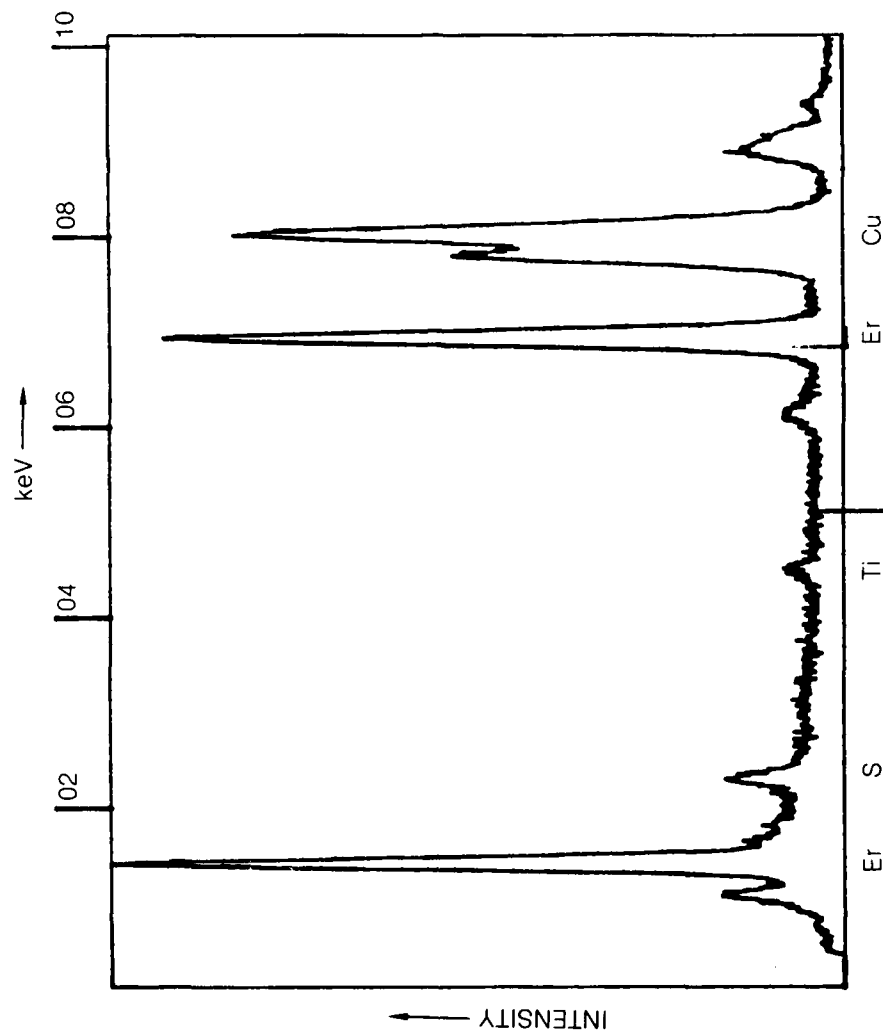
(B)  $Er\ L\alpha$  X-RAY IMAGE, AREA OF (A)



(C)  $Mo\ L\alpha$  X-RAY IMAGE, AREA OF (A)

FIG. 44

DISTRIBUTION AND EDS DATA,  $Er_2O_3$  IN SPECIMEN  
AS-LAYERGLAZED FROM Ti-6Al-2Sn-4Zr-6Mo POWDER

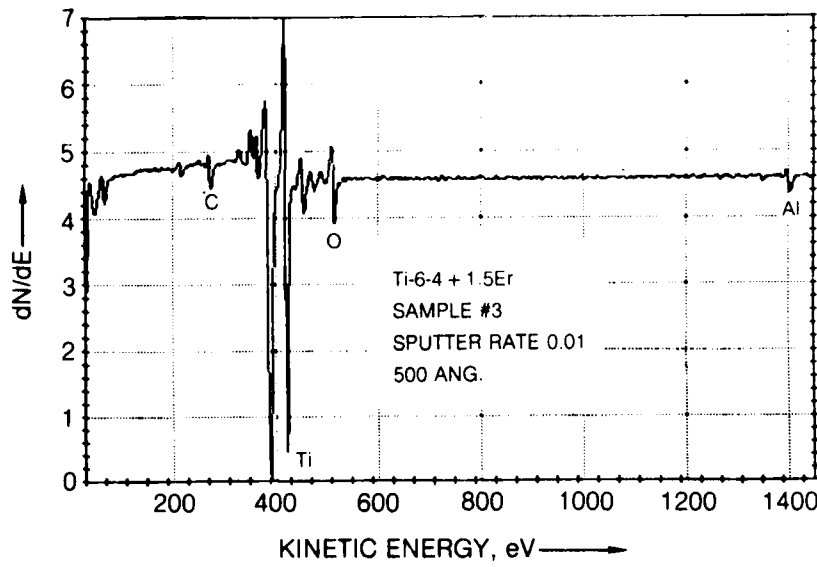


(A) CARBON EXTRACTION REPLICA. PARTICLE  
GIVING EDS DATA IN (B) MARKED BY ARROW

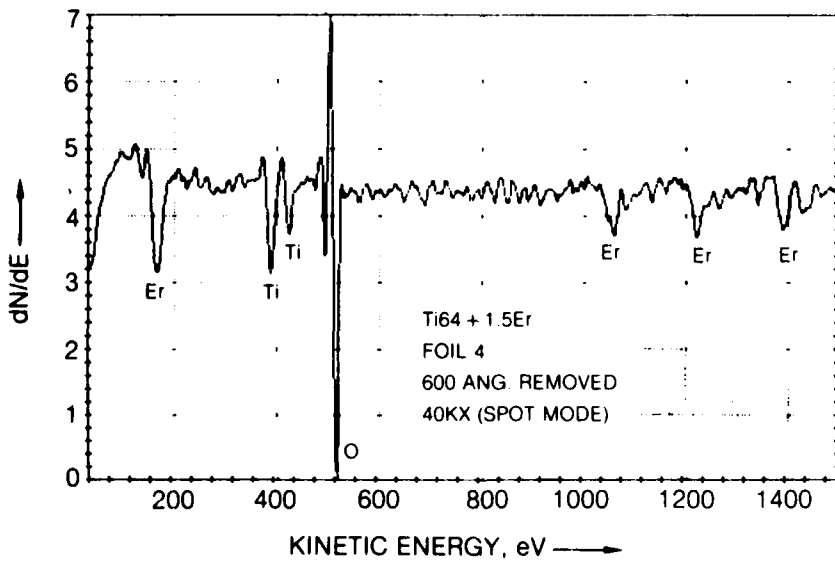
(B) ENERGY DISPERSIVE X-RAY SPECTRUM FROM INTERENDRITIC  $Er_2O_3$   
PARTICLE SHOWN BY ARROW IN (A). 120 kV, 5nm BEAM SPOT  
DIAMETER. Cu AND S PEAKS ARE ARTIFACTS

FIG. 45

**AUGER ELECTRON SPECTRA FROM SPECIMEN AS-LAYERGLAZED FROM  
Ti-6Al-4V-1.5Er, 100 nm BEAM DIAMETER**



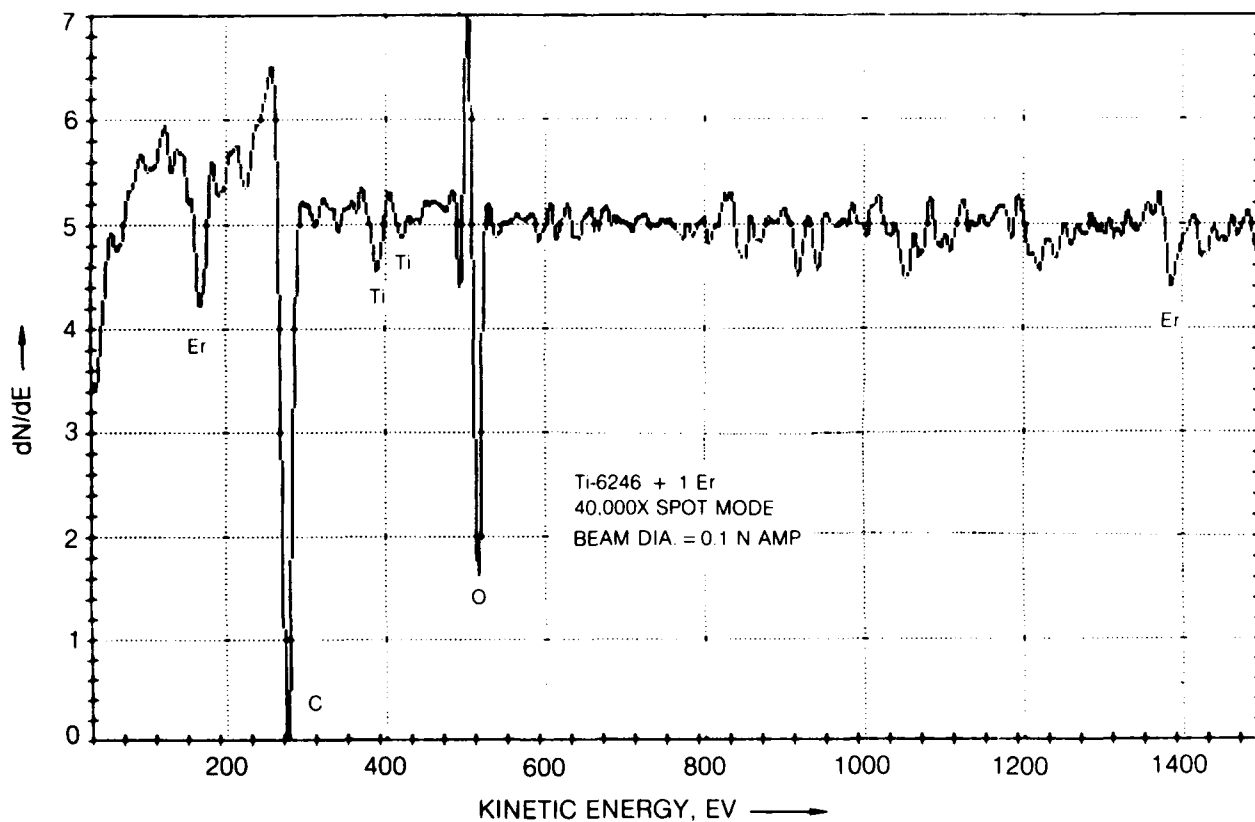
A)  $\alpha'$  HCP MARTENSITE



B) INTERDENDRITIC  $Er_2O_3$  PARTICLE

**AUGER ELECTRON SPECTRUM FROM CARBON EXTRACTION REPLICA, SPECIMEN AS-LAYERGLAGED FROM Ti-6Al-2Sn-4Zr-6Mo-1Er POWER.**

100nm BEAM DIAMETER



END

FILMED

DTIC